

A geochronologic framework for the Ziegler Reservoir fossil site, Snowmass Village, Colorado



Shannon A. Mahan^{a,*}, Harrison J. Gray^a, Jeffrey S. Pigati^b, Jim Wilson^c, Nathaniel A. Lifton^d, James B. Paces^e, Maarten Blaauw^f

^a U.S. Geological Survey, Denver Federal Center, Box 25046, MS-974, Denver, CO 80225, USA

^b U.S. Geological Survey, Denver Federal Center, Box 25046, MS-980, Denver, CO 80225, USA

^c Aeon Laboratories, LLC, 5835 N Genematas Dr, Tucson, AZ 85704-5919, USA

^d Department of Earth, Atmospheric, and Planetary Sciences, Purdue University, West Lafayette, IN 47907, USA

^e U.S. Geological Survey, Denver Federal Center, Box 25046, MS-963, Denver, CO 80225, USA

^f School of Geography, Archaeology and Palaeoecology, Queen's University Belfast, BT7 1NN Belfast, UK

ARTICLE INFO

Article history:

Received 30 September 2013

Available online 24 April 2014

Keywords:

Luminescence dating
Radiocarbon dating
Surface exposure dating
U-series dating
Ziegler Reservoir

ABSTRACT

The Ziegler Reservoir fossil site near Snowmass Village, Colorado (USA), provides a unique opportunity to reconstruct high-altitude paleoenvironmental conditions in the Rocky Mountains during the Last Interglacial Period. We used four different techniques to establish a chronological framework for the site. Radiocarbon dating of lake organics, bone collagen, and shell carbonate, and *in situ* cosmogenic ¹⁰Be and ²⁶Al ages on a boulder on the crest of a moraine that impounded the lake suggest that the ages of the sediments that hosted the fossils are between ~140 ka and >45 ka. Uranium-series ages of vertebrate remains generally fall within these bounds, but extremely low uranium concentrations and evidence of open-system behavior limit their utility. Optically stimulated luminescence (OSL) ages ($n = 18$) obtained from fine-grained quartz maintain stratigraphic order, were replicable, and provide reliable ages for the lake sediments. Analysis of the equivalent dose (D_e) dispersion of the OSL samples showed that the sediments were fully bleached prior to deposition and low scatter suggests that eolian processes were likely the dominant transport mechanism for fine-grained sediments into the lake. The resulting ages show that the fossil-bearing sediments span the latest part of Marine Oxygen Isotope Stage (MIS) 6, all of MIS 5 and MIS 4, and the earliest part of MIS 3.

Published by Elsevier Inc. on behalf of University of Washington.

Introduction

The unearthing of several bones of a juvenile Columbian mammoth in October 2010 during the expansion of Ziegler Reservoir, located near Snowmass Village, Colorado (Fig. 1), led to the discovery of one of the most prolific Pleistocene paleontological sites in North America. During the late Pleistocene, the site was occupied by a high-altitude lake that was bounded and underlain by till deposited during the Bull Lake glaciation, which has been dated elsewhere in the Rocky Mountains to ~200 to 130 ka (Blackwelder, 1915; Licciardi, 2000; Pierce, 2003). Lake sediments on top of the till are ~10 m thick, consist primarily of organic-rich silts and clays, and contain thousands of vertebrate and invertebrate fossils, as well as trees, logs, aquatic plants, invertebrates, plant macrofossils and pollen (Fig. 2).

To establish the ages of various sedimentary units at the site, and to date the fossils and environmental markers (directly or indirectly), we used four independent chronometric techniques: radiocarbon (¹⁴C),

surface exposure dating (*in situ* cosmogenic ¹⁰Be and ²⁶Al), uranium-series disequilibrium (U-series), and optically stimulated luminescence (OSL) dating. Radiocarbon dating constrains the age of carbon-bearing materials by measuring the time-dependent concentration of the unstable ¹⁴C isotope following plant or animal death (Hedges, 1981). Surface exposure dating using *in situ* cosmogenic radionuclides is used to determine the amount of time that a rock has been exposed at or near the ground surface by measuring rare isotopes that are produced by the interaction of cosmic radiation and target nuclei, mainly Si and O (Gosse and Phillips, 2001). U-series dating determines the age of materials that contain or uptake uranium, such as bone or calcium carbonate, by measuring isotopic concentrations of uranium, thorium, and associated daughter products (Ku, 2000).

In contrast to isotopic methods, OSL dating is not a function of a particular chemical element decay or buildup. Rather, it measures the growth of natural environmental radiation that results in trapped electron charged signals within a mineral grain that are eliminated by exposure to light or intense heat. The primary assumption involved in luminescence dating is that any residual signal from previous burial is removed by exposure to light (or in rare cases to heat) during transport, which would effectively “zero out” the luminescence clock (Aitken,

* Corresponding author.

E-mail address: smahan@usgs.gov (S.A. Mahan).



Figure 1. Site map with radiocarbon, cosmogenic (“cosmo”), and OSL sampling localities and “bone cloud” location.

1998; Rhodes, 2011). The potential for heterogeneous or incomplete bleaching is of foremost concern in any optical dating study involving glacial or lacustrine sediments (Fuchs and Owen, 2008). However, if transport pathways and burial conditions can be assessed based on sedimentologic or geomorphologic parameters, then luminescence dating can provide ages in a variety of geologic settings (Simms et al., 2011; Alexanderson and Murray, 2012; Bateman et al., 2012). Moreover, if dose rates are sufficiently low and luminescence signals in the sediments are stable, then the technique can provide reliable ages up to ~200 ka or more (Rhodes et al., 2006; Rhodes, 2011).

Materials and methods

Radiocarbon

We collected three sets of samples at the Ziegler Reservoir fossil site (ZRFS) for radiocarbon dating, including (1) wood, plant macrofossils, sedges, and shell fragments from the main exposures at localities 43, 51, and 52, (2) pieces of bone and tooth enamel from the Clay Mammoth at Locality 67, and (3) wood from near-shore sediments along the eastern margin of the reservoir at Locality 75 (Fig. 1). The analyzed

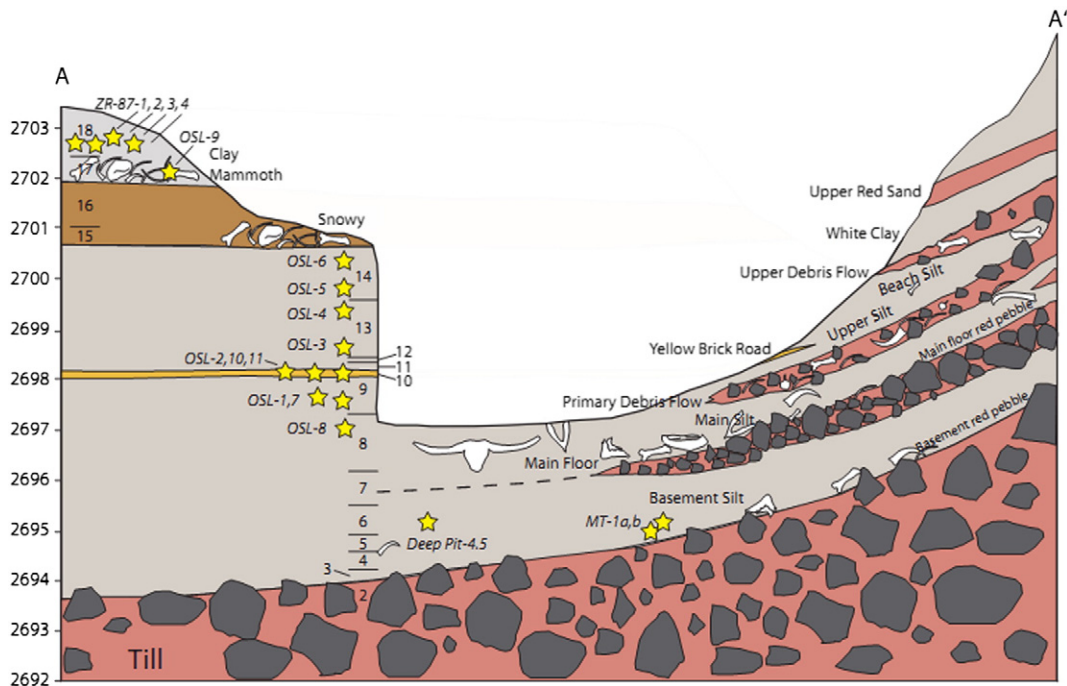


Figure 2. Stratigraphic section with labeled geological units (measured in meters), locations of significant fossil bone finds, and OSL sample locations highlighted as yellow stars.

organic samples were incredibly well preserved (Supplemental Fig. S.1). Pretreatment procedures varied by material and included the following:

- **Organics.** Most aliquots of wood, plant macrofossils, and sedges were subjected to the standard acid–base–acid (ABA) treatment to remove unwanted contaminants.
- **Collagen.** Dentin taken from within tooth enamel of the Clay Mammoth (Fig. 2; ZR11.60708) was crushed to <2 mm, washed in an ultrasonic bath of ultrapure water (ASTM Type I, 18.2 MΩ; UPW), rinsed with UPW until the water remained clear, and dried at room temperature under vacuum. Results of elemental analysis suggested that collagen suitable for ¹⁴C dating was present in the dentin (Table S.1, Supplemental information). The cleaned dentin was demineralized in 0.5 N HCl at room temperature. The resulting collagen residue was washed in a 0.1 N NaOH solution, and then denatured into gelatin in 0.01 N HCl at 60°C. The high molecular weight fraction of the gelatin was concentrated by ultrafiltration using a 30 kDa molecular weight cutoff, and dried in a vacuum centrifuge.
- **Humic acids.** The nitrogen content of the cortical bone from a radius of the Clay Mammoth (Fig. 2; ZR11.67.3) indicated that collagen suitable for ¹⁴C dating was not present in this sample. Further analysis indicated that the organic compounds present consisted primarily of humic acids, which were extracted, precipitated, rinsed, and dried for analysis with the goal of establishing at least a minimum age for the specimen.
- **Shell carbonate.** Shell fragments of aquatic gastropods collected near the base of Unit 18 at Locality 51 were sonicated in UPW and then treated with hot 3% H₂O₂ to remove any persistent organic residues. After rinsing, shell fragments were leached in dilute HCl to remove secondary carbonates. The leached material was then rinsed in UPW and dried.
- **Untreated.** Two wood samples, ZR11.49.8 (–20) and ZR11.ALJW.1, and bone powder from the Clay Mammoth radius (Fig. 2) were washed in UPW but otherwise remained untreated.

After pretreatment, materials were either combusted in the presence of excess O₂ (organics) or digested in H₃PO₄ (shell carbonate). The resulting CO₂ was purified using a combination of cryogenic and

high-temperature copper and silver wool traps, and the yield was measured manometrically. A small aliquot was taken for stable isotope analysis (δ¹³C). The remainder was converted to graphite by hydrogen reduction over an iron catalyst and analyzed for ¹⁴C activity by accelerator mass spectrometry (AMS). Finite ¹⁴C ages were calibrated using the IntCal09 dataset and CALIB 6.0 (Stuiver and Reimer, 1993; Reimer et al., 2009). Ages are presented in thousands of calibrated ¹⁴C yr BP (Before Present; 0 cal yr BP = AD 1950) unless otherwise noted, and uncertainties are given at the 95% (2σ) confidence level (Table 1).

In situ cosmogenic radionuclides

A small moraine bounds the ZRFS to the north, east and south. It was formed when a large glacier overtopped a low spot on the east side of Snowmass Creek Valley west of the site (Fig. 1; see Pigati et al., 2014–in this volume, for details on the geologic setting). A second moraine cuts off this bounding moraine on the northwestern side of the basin. Both have crests varying 5–10 m in width, but locally they exhibit crests up to 30 m wide. The crests of both moraines were searched for boulders suitable for surface exposure dating by *in situ* cosmogenic ¹⁰Be and ²⁶Al. Only one large granitic boulder was found in a stable position on the crest, on a ~30-m-wide portion of the northeastern section of the bounding moraine (Figs. 1, 3a). The boulder is positioned several meters below a sharper-crested zone to the northwest on the moraine, indicative of erosion in the area. Other boulders were present, but were either small (less than ~25 cm in height) or positioned on unstable, sloping surfaces.

The sampled boulder (ZR11-BL0) was 1.7 m × 1.1 m × 0.4 m high, and was very dense, ringing when hit with a hammer, which suggests a lack of burial and weathering. Samples were collected by breaking off parts of the upper 1–2 cm of the top surface of the boulder using a hammer and chisel (Fig. 3b). The sample location was measured with a handheld GPS, and the altitude was tied to the detailed survey of the excavation (Lucking et al., 2012).

A depth profile was also sampled from a soil pit dug adjacent to the surface boulder to augment chronologic information from that single *in situ* cosmogenic nuclide sample and to constrain surface erosion

Table 1
Summary of sample information, carbon-14 ages, and calibrated ages.

Sample #	Lab ID	Material dated	Unit	Treatment	Yield	δ ¹³ C (vpdb)	F ¹⁴ C	¹⁴ C age (¹⁴ C ka BP)	Age (cal ka BP) ¹	P ²
<i>Clay Mammoth</i>										
ZR11.60708	Aeon-981	Dentin collagen	18	Ultrafiltration	45.0%	–19.8	0.0032 ± 0.0008	46.20 ± 1.90	– ³	
ZR11.67.3a	Aeon-833	Bone powder	18	None	2.2%	–16.3	0.1146 ± 0.0016	17.40 ± 0.11	20.77 ± 0.45	1.00
ZR11.67.3b	Aeon-844	Humic acids	18	ABA	36.2%	–28.0	0.0949 ± 0.0012	18.92 ± 0.10	22.61 ± 0.37	0.94
									23.18 ± 0.06	0.06
<i>Lake-center sediments</i>										
ZR10.51.18.193-201	Aeon-705	Shell fragments ⁴	18	Acid leach	11.1%	–11.4	0.0040 ± 0.0009	44.30 ± 1.90	– ³	
ZR10.43.16.275	Aeon-663	Peat	16	ABA	41.6%	–9.6	0.0032 ± 0.0009	46.30 ± 2.40	– ³	
ZR10.51.16.113	Aeon-664	Wood	16	ABA	54.9%	–22.7	0.0002 ± 0.0009	>49.3	–	
ZR10.43.13.85	Aeon-662	Wood	13	ABA	51.4%	–22.5	0.0010 ± 0.0009	>47.3	–	
ZR10.43.12.44	Aeon-661	Sedges	12	ABA	47.5%	–13.9	0.0012 ± 0.0009	>46.7	–	
ZR10.43.10.17	Aeon-660	Wood	10	ABA	50.9%	–24.6	0.0015 ± 0.0009	>45.9	–	
ZR10.52.9b. (–21)	Aeon-659	Plant macrofossil	9b	ABA	54.7%	–23.3	0.0002 ± 0.0009	>49.3	–	
ZR10.52.9a. (–39)	Aeon-658	Plant macrofossil	9a	ABA	48.0%	–20.5	0.0021 ± 0.0009	49.30 ± 3.50	– ³	
ZR10.52.8. (–123)	Aeon-657	Wood	8	ABA	54.5%	–23.0	0.0023 ± 0.0009	48.60 ± 3.00	– ³	
<i>Near-shore sediments</i>										
ZR11.ALJW.1a	Aeon-819	Wood	White clay	None	33.3%	–22.7	0.0073 ± 0.0009	39.49 ± 0.96	43.6 ± 1.4	1.00
ZR11.ALJW.1b	Aeon-821	Wood	White clay	ABA	37.2%	–23.9	0.0062 ± 0.0009	40.80 ± 1.10	44.5 ± 1.6	1.00
ZR11.49.8. (–20)a	Aeon-818	Wood	Main silt	None	35.0%	–22.0	0.0009 ± 0.0009	>47.7	–	
ZR11.49.8. (–20)b	Aeon-820	Wood	Main silt	ABA	34.2%	–22.3	0.0004 ± 0.0009	>48.9	–	

¹ Calibrated ages were calculated using CALIB v. 6.0.0, IntCal09.14C dataset; limit 50.0 calendar ka BP. Calibrated ages are reported as the midpoint of the calibrated range. Uncertainties are calculated as the difference between the midpoint and either the upper or lower limit of the calibrated age range, whichever is greater (reported at the 95% confidence level; 2σ).

² P = probability of the calibrated age falling within the reported range as calculated by CALIB.

³ Exceeds the 50.0 calendar ka limit of the IntCal09.14C dataset.

⁴ Shells identified in this stratum included the aquatic gastropod *Stagnicola caperata* and bivalves *Sphaerium rhomboideum* and *Pisidium milium*. The aliquot measured here likely included fragments of all three taxa.

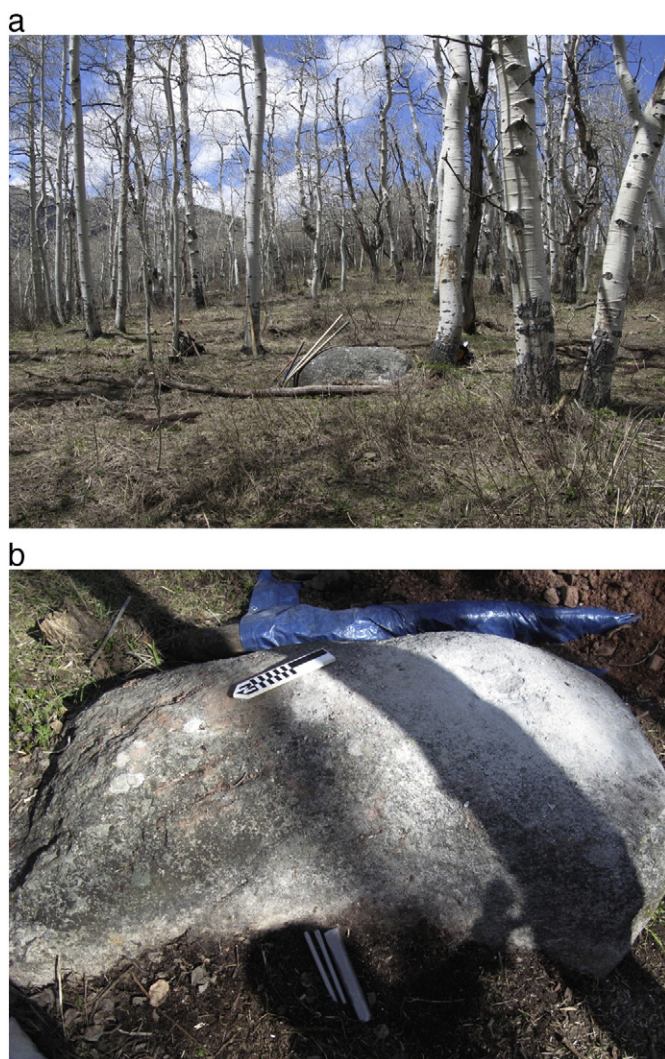


Figure 3. (a) Photograph of cosmogenic sampling site for ZR11-BLO ("Cosmo boulder" in Fig. 1), looking northwest up the moraine crest, (b) close up photograph of sampled boulder ZR11-BLO.

magnitude. Seven quartzite and well-indurated conglomeratic cobbles likely from the Maroon Formation were sampled from depths ranging from 28 to 91 cm below ground surface for ^{10}Be and ^{26}Al analysis (Supplemental Table S.2).

In the laboratory, each sample was first crushed and sieved to 250–500 μm . Quartz was then isolated using procedures modified from those of Kohl and Nishiizumi (1992). After checking the resulting purity by measuring Al concentrations *via* inductively coupled plasma-optical emission spectroscopy (ICP-OES) (Table 2), the sample was dissolved and Be and Al were isolated using standard cation and anion exchange column procedures (Strelow et al., 1972; Ochs and Ivy-Ochs, 1997). The resulting Be and Al hydroxides were combusted to BeO and Al $_2\text{O}_3$, mixed with Nb and Ag powders, respectively, and pressed into target holders for analysis by accelerator mass spectrometry (AMS) at PRIME Lab.

Surface exposure ages from each nuclide were calculated using the CRONUS-Earth online calculator (<http://hess.ess.washington.edu/math/>) (Balco et al., 2008). We assumed that the boulder was exposed continuously since the ice retreated from the moraine on which it sits, with no erosion of the boulder nor inherited inventories from a prior exposure event. We utilized the time-dependent Lal (1991)/Stone (2000) (L_m) scaling model for this discussion, and corrected production rates for attenuation by snow cover at the site based on the National

Resources Conservation Service's SNOwpack TELEmetry (SNOTEL) data in the vicinity from 1981 to 2010 (<http://www.wcc.nrcs.usda.gov/snotel/Colorado/colorado.html>) (Table 2, Supplemental Fig. S.2, and Supplemental Tables S.2 and S.3).

Uranium series

A variety of samples were selected to evaluate the U–Th characteristics of excavated bone and the viability of the U-series dating method on these materials. Specimens came from a number of stratigraphic horizons including Unit 15, Primary Debris Flow, Beach Silt, Main Silt, and Basement Silt (Table 3; Fig. 4). Samples included limb bones from large animals (mammoth, mastodon, and bison), skulls, horn-core, and tusks, as well as whole bone or bone fragments from small animals (salamander and rabbit). Large bones were sectioned and polished so that multiple subsamples could be taken at varying distances from outer and inner surfaces of compact layers. Smaller bones were cleaned in an ultrasonic bath of deionized water prior to removal of remaining detrital material or fragments that looked degraded under binocular magnification using dental burs. Secondary mineralization of compact bone was minimal as most retained a strong odor of burning organic material when carbide or diamond grinding tools were used. Photographs of samples along with locations of analyzed subsamples are included in the Supplemental information (Supplemental Figs. S.5 to S.15).

In addition to bone, two samples of groundwater were collected from seeps flowing out of the walls or floors of active excavations. Sample ZR-1-HOH was collected on June 21, 2011 from a seep flowing at $\sim 0.03 \text{ l s}^{-1}$ out of the Basement Silt unit southeast of Locality 43 (Fig. 1). Sample ZR-3-HOH was collected on the same day out of a freshly dug pit in the uppermost clayey units at Locality 79 from a seep flowing at $\sim 0.08 \text{ l s}^{-1}$. Both samples consisted of fresh, clear discharge with no likelihood of contamination by surface flow.

Small amounts of coarsely crushed or powdered bone sample ranging from 0.064 to 0.313 g were weighed in perfluoroalkoxy (PFA) teflon vials and spiked with known amounts of a mixed-isotope tracer solution (^{236}U – ^{233}U – ^{229}Th). Samples were digested using inorganic acids ($\text{HNO}_3 + \text{HCl}$). U and Th were separated from digested solutions and purified using standard ion chromatographic methods using AG1 \times 8 (200–400 mesh) anion resin. Total process blanks, measured along with samples, were approximately 20 pg for U and 100 pg for Th and Sr.

Resulting U salts were loaded on rhenium (Re) side filaments as part of double-filament assemblies. Th salts were loaded along with graphite suspension on single Re-filament assemblies. Isotope ratios were obtained on a Thermo Finnigan Triton thermal ionization mass spectrometer (TIMS) equipped with an RPQ electrostatic filter¹. U-series isotope ratios ($^{234}\text{U}/^{238}\text{U}$, $^{236}\text{U}/^{235}\text{U}$, $^{230}\text{Th}/^{229}\text{Th}$, and $^{232}\text{Th}/^{229}\text{Th}$) were determined using a single ETP electron multiplier operating in peak-jumping mode. $^{234}\text{U}/^{238}\text{U}$ isotopic compositions of National Institute of Standards & Technology (NIST) 4321B standard determined over the same time period yielded results within analytical uncertainty of the certified value (0.007294 ± 0.000028). Results for a U.S. Geological Survey (USGS) in-house secular equilibrium standard yielded an average $^{234}\text{U}/^{238}\text{U}$ activity ratio (AR) of 0.9984 ± 0.0025 (2σ) and an average $^{230}\text{Th}/^{238}\text{U}$ activity ratio (AR) of 0.993 ± 0.046 (2σ). Both values should be 1.000 for a material in radioactive secular equilibrium.

$^{230}\text{Th}/\text{U}$ ages were calculated from measured $^{230}\text{Th}/^{238}\text{U}$ AR and $^{234}\text{U}/^{238}\text{U}$ AR data after correction for the presence of initial ^{230}Th and ^{234}U . Corrections were based on the assumption that (1) ^{232}Th is insoluble in near-surface aqueous solutions and (2) any ^{232}Th measured in the samples is the result of transport of a non-authigenic (detrital)

¹ Any use of trade, product, or firm names is for descriptive purposes only and does not imply endorsement by the U.S. Government.

Table 2
In situ cosmogenic sample data and results.

Sample number	PRIME ID	Location (°N/°E)	Altitude (m asl)	Thickness (cm)	Shielding factor ¹	Quartz (g)	Be carrier (g) ²	¹⁰ Be/ ⁹ Be (×10 ⁻¹³)	[¹⁰ Be] (10 ⁶ at g ⁻¹) ³	¹⁰ Be Age (ka) ⁴	²⁶ Al/ ²⁷ Al (×10 ⁻¹³)	[²⁶ Al] (10 ⁶ at g ⁻¹) ³	²⁶ Al Age (ka) ⁴
ZR11-BLO	201101968	39.20865/ -106.96278	2720	2	0.938	30.67	0.265	69.5 ± 1.5	4.29 ± 0.10	138 ± 12 158 ± 9	130 ± 4	26.36 ± 0.81	129 ± 12 149 ± 9

Note: Assumed density of 2.65 g cm⁻³ due to granitic composition, and no erosion, yielding a minimum age. Uncertainties reported at 1σ level. Propagated uncertainties include error in blank, carrier mass, and counting statistics. Age uncertainties include production rate uncertainties.

¹ Topographic shielding factor of 0.993 calculated using the CRONUS-Earth geometric shielding calculator (http://hess.ess.washington.edu/math/general/skyline_input.php) combined with a 0.945 snow cover correction. Mean snow water equivalent (SWE) depths from Natural Resources Conservation Service (<http://www.wcc.nrcs.usda.gov/snotel/Colorado/colorado.html>) SNOTEL sites for 1981–2010. Sites are: Nast Lake (2652 m altitude), North Lost Trail (2804 m altitude), Kiln (2926 m altitude), and Ivanhoe (3170 m altitude). Mean SWE depth = 9.1 cm. Snow cover correction assumes an exponential decrease in *in situ* production with increasing SWE depth, governed by an attenuation length of 160 g cm⁻² and a water density of 1.0 g cm⁻³.

² Be concentration in carrier solution is 1069 ppm.

³ No Al carrier added. Stable Al concentration in the quartz sample was 4.86 ppm (±2%) by ICP-OES. ¹⁰Be and ²⁶Al isotope ratios normalized to ¹⁰Be and ²⁶Al standards prepared by Nishiizumi et al. (2007) (¹⁰Be/⁹Be = 6.320 × 10⁻¹²) and Nishiizumi (2004) (²⁶Al/²⁷Al = 4.694 × 10⁻¹²), respectively, using ¹⁰Be and ²⁶Al mean lives of 2.005 Ma and 1.02 Ma, respectively. A procedural blank of 6.47 ± 2.50 × 10⁵ at/g carrier (0.2149 g, ¹⁰Be/⁹Be = 9.06 ± 3.49 × 10⁻¹⁵) was used for background correction. Procedural blank for ²⁶Al was not detectable.

⁴ Top row of Be and Al model ages calculated using CRONUS-Earth online calculator (Balco et al., 2008), version 2.2, with scaling model Lm using “global” spallogenic sea level, high latitude (SLHL) production rate for ¹⁰Be – value for Lm is 4.39 ± 0.37 ¹⁰Be at g⁻¹ yr⁻¹. Bottom row (italicized) model ages calculated using a modified CRONUS-Earth calculator with scaling model Lm (time-dependent Lal (1991)/Stone (2000)) using Northeastern North America ¹⁰Be spallogenic SLHL production rate of Balco et al. (2008), restandardized to Nishiizumi et al. (2007). Value for Lm is 3.85 ± 0.19 ¹⁰Be at g⁻¹ yr⁻¹. Muogenic production rates from Heisinger et al. (2002a,b) as implemented by Balco et al. (2008). Al SLHL production rates assume ¹⁰Be/²⁶Al production ratio of 6.75.

component that also contributes initial ²³⁰Th and ²³⁴U not generated by *in situ* decay (Ludwig and Titterton, 1994; Ludwig and Paces, 2002). Values assumed for the isotopic composition of the detrital component are given in Table 3. Analyses were corrected for detrital contributions only when U concentrations were >0.05 μg/g (ppm) and Th concentrations were relatively small (²³²Th/²³⁸U AR <1.0). In cases where these conditions were met (10 out of 28 analyses), finite ²³⁰Th/U ages and initial ²³⁴U/²³⁸U AR values were calculated using the conventional iterative solution to the ²³⁰Th/U age equations (Ivanovich and Harmon, 1992; Ludwig, 2003). Multiple analyses of an in-house late Pleistocene *Acropora* coral dating standard (preferred age of 119.6 ± 1.9 ka; Watanabe and Nakai, 2006) yielded an average ²³⁰Th/U age of 118.3 ± 3.5 ka (2σ, n = 25) and an average initial ²³⁴U/²³⁸U AR value of 1.152 ± 0.004, which is within error of the modern seawater value of 1.1496 ± 0.0060 (Delanghe et al., 2002).

Luminescence

Samples for luminescence dating were collected using three different methods based on availability, access, and sample type.

- **Outcrops.** Sediments exposed in outcrop at localities 43, 51, and 52 (Fig. 1) were collected using standard procedures involving thick-walled tubes. Prior to sampling, we removed at least 50 cm of sediment from the face of each exposure to minimize the possibility of modern or accidental bleaching of the sediments. Solid black cloth shielding was used while opaque polyvinyl chloride (PVC) tubes, ~20 cm long and 6 cm in diameter, were hammered perpendicular into the exposed vertical faces to extract the sediment samples (Fig. 5). In the USGS luminescence laboratory in Denver, CO, we removed at least 5 cm of sediment from both ends of the OSL sampling tube under “safe light” conditions (sodium vapor lighting) prior to analysis.
- **Tusks.** Sediments trapped inside mammoth and mastodon tusks were sampled at the Denver Museum of Nature and Science (DMNS) under dark-room conditions. These samples were stored in film canisters and were entirely utilized since they were collected in near total darkness.
- **Blocks.** Opaque, solid blocks of sediment that were at least 6 cm in diameter were collected from DMNS storage facilities. The block surfaces were spray painted shortly after collection and transported to the laboratory for further processing. Then we extracted 2-cm-diameter cores from the center of the blocks under safe light conditions.

Equivalent dose (D_E) calculations

Quartz OSL ages, using blue-light diode stimulation, were determined on fine sand-size (63–90 μm) quartz separates using single aliquot regeneration (SAR) protocols with continuous wave optically stimulated luminescence (CW-OSL). We also determined luminescence ages on the polymineralic fine silt fraction (4–11 μm) using infra-red stimulated luminescence (IRSL) techniques on potassium feldspars. Details are given in the Supplemental information (Figs. S.16 to S.46 and Tables S.5 and S.6).

The SAR-OSL procedure involved the measurement of the natural OSL signal (L_N) and successive regenerated OSL signals (L_X) for each grain analyzed. The latter are used to construct a dose–response curve, onto which L_N is projected to determine the D_E. The SAR procedure included the use of a 40-second blue-light diode wash step (Murray and Wintle, 2003) at the same temperature as the preheat step and the preferred component of SAR dating (the “fast” component; Wintle and Murray, 2006; Rhodes, 2011), a signal usually released in the first 1 s of a typical blue diode stimulation. The SAR protocol was used because precision of ~10% (and sometimes less) can be attained routinely with multigrain SAR quartz methods (Murray and Olley, 2002; Lian and Roberts, 2006; Duller, 2008) when applied to almost any sediment type (Rhodes, 2011). All sample aliquots were analyzed at temperatures of 125°C after 10 second preheats between 240 and 260°C. These temperatures were based on in-house experiments and prior results with samples of similar age and lithology (Duller, 2008).

We evaluated the veracity of the SAR protocol using multiple tests to ensure that the sediments from the ZRFS were responsive to the optical techniques and that proper preheat temperatures were used. These tests included: the recycling ratio, recuperation, IR repeat ratio, dose recovery, preheat plateau, and the D_E (t) distribution (Duller, 2008). Samples that failed any of these tests, exhibited unstable OSL signals, or did not yield SAR equivalent dose values were excluded from further analysis. Data rejection criteria followed standard protocols used by the luminescence dating community (Wintle and Murray, 2006; Rhodes, 2011). In addition, D_E distributions of >15% correlated with the presence of coarse-grained sediments derived from the adjacent moraine via mass wasting processes; ages derived from such samples were also excluded from the final chronology.

The growth of the luminescence signal (Fig. 6a) by increasing the laboratory dose was well represented by a single saturating exponential plus linear function and illustrates the generally reliable behavior of the ZRFS quartz samples for the SAR protocol by forcing

Table 3
Measured uranium and thorium concentrations and isotope compositions, along with calculated detritus-corrected U-series isotope ratios, ²³⁰Th/U ages, and initial ²³⁴U/²³⁸U activity ratios for bone and groundwater samples.

Sample name	Stratigraphic unit	Sample type	Description or distance from outer surface	Weight (g)	U conc. (µg/g)	Th conc. (µg/g)	Measured activity ratios ¹				Detritus-corrected activity ratios ²			²³⁰ Th/U age ± 2σ (ka) ³	Initial ²³⁴ U/ ²³⁸ U AR ± 2σ ³	ρ _{age-γ0}
							²³² Th/ ²³⁸ U AR (± 2σ)	²³⁰ Th/ ²³⁸ U AR (± 2σ)	²³⁴ U/ ²³⁸ U AR (± 2σ)	²³⁰ Th/ ²³² Th AR (± 2 s)	²³⁰ Th/ ²³⁸ U AR (± 2σ)	²³⁴ U/ ²³⁸ U AR (± 2σ)	ρ ₄₈₋₀₈			
60676-F1	Unit 15	Mammoth femur section	0–2 mm	0.223	0.081	0.481	1.945 ± 0.006	1.37 ± 0.02	1.669 ± 0.008	0.7						
60676-F2			2–4 mm	0.138		0.064	No U isotope data				1.0					
60676-F3			4.5–7.0 mm	0.313	0.014	4.60	110.8 ± 1.4	29.1 ± 1	1.96 ± 0.04	0.3						
60676-F4			7.0–9.0 mm	0.174	0.012	0.086	2.45 ± 0.04	3.26 ± 0.17	1.8 ± 0.1	1.3						
60676-F6			12.5–15 mm	0.229	0.013	0.100	2.63 ± 0.05	3.09 ± 0.08	2.46 ± 0.11	1.2						
60676-F8			19–22 mm	0.281	0.010	0.118	3.75 ± 0.08	2.19 ± 0.1	1.61 ± 0.05	0.6						
60676-T1	Unit 15	Mammoth tusk	Fragments	0.204	0.044	0.311	2.33 ± 0.02	1.33 ± 0.03	1.68 ± 0.04	0.6						
60679a	Unit 15	Bison femur section	Outer 2 mm	0.129	0.061	0.090	0.485 ± 0.007	1.68 ± 0.03	1.48 ± 0.06	3.5	2.10 ± 0.37	1.78 ± 0.26	0.82	Excess ²³⁰ Th	Not calculated	
60679b			Outer 2 mm	0.124	0.146	0.078	0.176 ± 0.001	0.607 ± 0.011	1.412 ± 0.013	3.4	0.544 ± 0.056	1.478 ± 0.044	−0.57	49 ± 7	1.55 ± 0.04	−0.59
60679c			Inner 2 mm	0.156	0.321	2.08	2.135 ± 0.008	1.41 ± 0.02	1.447 ± 0.006	0.7						
69.114a	Beach Silt	Salamander vertebrae	Multi-bone	0.064	5.21	9.47	0.599 ± 0.003	1.098 ± 0.006	1.221 ± 0.004	1.8	1.18 ± 0.24	1.42 ± 0.20	0.31	169* ± 78	1.67** ± 0.29	−0.03
60680-A1	Primary	Mastodon	0–2 mm	0.151	0.063	0.0676	0.355 ± 0.003	0.497 ± 0.016	1.33 ± 0.02	1.4	0.30 ± 0.17	1.46 ± 0.10	−0.71	25 ± 17	1.49 ± 0.09	−0.65
60680-A2	Debris Flow	femur section	3–4 mm	0.164	0.020	2.08	35.2 ± 0.3	6 ± 0.2	1.43 ± 0.03	0.2						
60680-A3			5–7.5 mm	0.170	0.006	11.18	579 ± 14	459 ± 12	1.6 ± 0.05	0.8						
60680-A5			12–16 mm	0.172	0.020	0.104	1.718 ± 0.016	2.29 ± 0.07	1.76 ± 0.13	1.3						
60681A	Unknown	Mastodon tusk	Inner 11–20 mm	0.180	0.005	0.0941	6.3 ± 0.3	88 ± 5	0.89 ± 0.06	14.0						
60681B			Inner 25–33 mm	0.209	0.006	0.120	7.17 ± 0.13	173 ± 3	No ²³⁴ U data	24.1						
60720a	Primary Debris Flow	Bison horn core	Fragment	0.250	0.053	0.104	0.648 ± 0.005	0.89 ± 0.02	1.43 ± 0.03	1.4	0.78 ± 0.29	1.86 ± 0.46	−0.38	56* ± 37	2.01** ± 0.47	−0.66
60720b			Fragment	0.292	0.067	1.46	7.22 ± 0.04	2.17 ± 0.04	1.372 ± 0.014	0.3						
48.018a	Main Silt	Bison horn core	Fragment	0.172	0.042	0.073	0.58 ± 0.04	No data	1.4 ± 0.02							
48.018b			Fragment	0.203	0.707	0.122	0.057 ± 0.002	0.78 ± 0.19	1.467 ± 0.011	13.7	0.767 ± 0.195	1.489 ± 0.017	−0.02	75 ± 26	1.61 ± 0.05	0.90
54.260a	Main Silt	Salamander vertebrae	Multi-bone	0.205	0.675	0.131	0.0638 ± 0.0004	0.551 ± 0.008	1.455 ± 0.015	8.6	0.527 ± 0.020	1.479 ± 0.021	−0.38	47 ± 3	1.55 ± 0.02	−0.53
72.127a	Basement Silt	Rabbit femur	Fragment	0.148	8.60	6.73	0.2577 ± 0.0011	0.837 ± 0.004	1.46 ± 0.004	3.2	0.796 ± 0.069	1.576 ± 0.077	−0.36	73 ± 11	1.71 ± 0.08	−0.56
82.148a	Basement Silt	Mastodon tooth	Outer enamel	0.065	2.39	0.184	0.0254 ± 0.0001	0.943 ± 0.005	1.454 ± 0.004	37.2	0.942 ± 0.007	1.463 ± 0.007	−0.06	104.4 ± 1.6	1.62 ± 0.01	−0.31
82.148b			Inner enamel	0.155	0.001	0.011	2.5 ± 0.7	12 ± 0.7	1.71 ± 0.1	4.8						
82.148c				0.281	0.009	0.007	0.26 ± 0.03	8.6 ± 0.7	1.37 ± 0.23	33						
82.148d			Dentin	0.176	0.277	0.010	0.0119 ± 0.0004	1.25 ± 0.02	1.47 ± 0.03	105	1.25 ± 0.022	1.476 ± 0.031	0.00	171** ± 11	1.77** ± 0.03	−0.50
82.148e			Dentin	0.082	0.288	0.034	0.0385 ± 0.0009	2.3 ± 0.04	1.47 ± 0.03	60	2.345 ± 0.049	1.479 ± 0.036	0.09	Excess ²³⁰ Th	Not calculated	
ZR-1-HOH	Basement Silt	Groundwater			0.00031				1.787 ± 0.005							
ZR-3-HOH	Unit 15	Groundwater			0.00057				1.542 ± 0.004							

¹ Measured isotope ratios corrected for mass fractionation, spike contributions, procedural blank & normalized relative to a value for NIST SRM 4321b ²³⁴U/²³⁸U = 0.0000529.

² Detritus-corrected activity ratios calculated for samples with U concentrations >0.05 µg/g and ²³²Th/²³⁸U AR <1.0. Assumed Th-bearing detrital component has an atomic Th/U of 4 with the following activity ratios and 2 s errors: ²³²Th/²³⁸U AR = 1.276 ± 0.64; ²³⁴U/²³⁸U AR = 1.0 ± 0.1; and ²³⁰Th/²³⁸U AR = 1.0 ± 0.25. ρ₄₈₋₀₈ = error correlation between ²³⁴U/²³⁸U and ²³⁰Th/²³⁸U ratios.

³ ²³⁰Th/U age, initial ²³⁴U/²³⁸U ratio and associated errors calculated using detritus-corrected activity ratios. ρ_{age-γ0} = error correlation between age and initial ²³⁴U/²³⁸U ratio.

* Large uncertainties due to initial ²³⁰Th correction. Calculated age and initial ratio are considered unreliable.

** Data show evidence of open-system behavior. Calculated age and initial ²³⁴U/²³⁸U AR are considered unreliable.

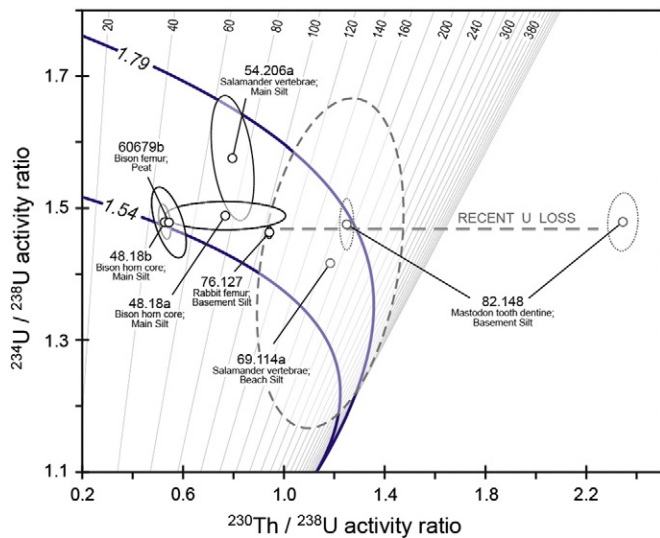


Figure 4. U-series isotope evolution plot showing centroids and error ellipses for analyses of ZRFS bones corrected for the presence of initial ^{230}Th using criteria discussed in the text and Table 3. Thick blue curves represent compositional evolution paths of $^{234}\text{U}/^{238}\text{U}$ and $^{230}\text{Th}/^{238}\text{U}$ isotopes under closed conditions (no loss or gain of mass since the time of formation) for starting U-isotope compositions measured in ZRFS groundwater ($^{234}\text{U}/^{238}\text{U}$ AR of 1.54 and 1.79). Straight sloping lines are isochrons given at 20 ka intervals.

the dose–response curves through the origin (Fig. 6b). Rodnight (2008) suggested that at least 50 measured aliquots per sample are preferable; we determined that 20 to 30 aliquots per sample were sufficient at the ZRFS owing to the low dispersion of D_E data (Figs. 7a, b, and c).

We then applied statistical indices of mean, median, standard deviation, standard error, and scatter (over-dispersion) in the D_E measurements, and applied the central age model (CAM) as well as the minimum age model (MAM) (Galbraith et al., 1999) when needed. The experimental results did not show evidence of partial bleaching, and the over-dispersion for samples within the ZRFS sediments was low (generally <15%). Thus, the CAM protocol was favored, as the MAM protocol may have underestimated the ages because of the tight D_E distributions (Duller, 2008; Rhodes, 2011). The finite mixture model is generally considered to be the most useful for fluvial sediments (Galbraith and Green, 1990).

Dose rate (D_R) calculations

We employed four separate methods to determine dose rates at the ZRFS, including two chemical methods: inductively coupled plasma mass spectrometry (ICP-MS) and instrumental neutron activation analysis (INAA), and two differing radiation dosimetry techniques: *in situ* gamma emission counting using a sodium iodide (NaI) detector and high resolution gamma spectrometry with a high purity germanium (HPGe) detector following the procedures described in Snyder and Duval (2003).

ICP-MS and INAA analysis were performed at the USGS analytical chemistry facilities in Denver CO. ICP-MS was performed for all samples and INAA was performed as a check for ICP-MS for samples ZR.OSL-1 through ZR.OSL-11. Measured elemental concentrations, associated dose rates, and cosmic ray contributions are presented in Table 4. The cosmic-ray dose rate was estimated for each sample as a function of depth, altitude and geomagnetic latitude and added to the total dose rate (Prescott and Hutton, 1994). Alpha and beta contributions to the dose rate were corrected for grain-size attenuation (Aitken, 1985). The alpha efficiency for the silt-sized samples was determined by comparing multiple aliquot additive dose (MAAD)-alpha source exposed and MAAD-beta source exposed curves, using approaches in Aitken (1985).

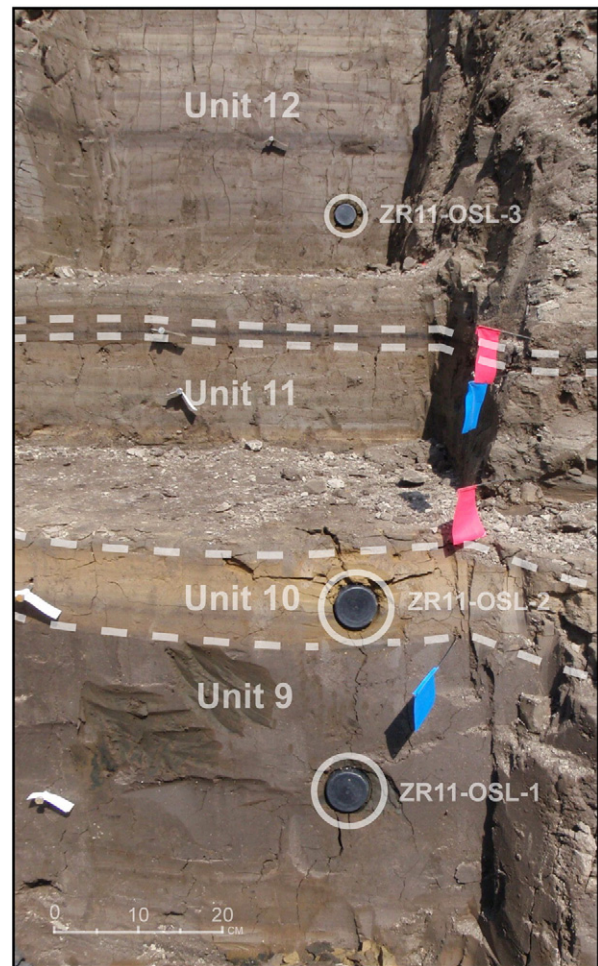


Figure 5. Photograph of OSL sampling at Locality 43 with tubes in sediment. Yellow horizontal bed (Unit 10) is the oxidized lake bed used as a stratigraphic tie point between lake-center and near-shore sediments.

In situ measurements for samples taken at localities 43, 51, and 52 were performed to accurately capture the gamma dose rate in the field (Duller, 2008). A probe was inserted into a position as close as possible to the exact location of sample collection using an Exploranium GR-256 Gamma Spectrometer fitted with a 33 cm × 11.5 cm probe. The probe was completely buried into an augured hole at each site and counted for an average of 35 min per sample. Individual U, Th, and K concentrations were taken from the peaks of ^{40}K , ^{214}Bi (as a proxy for U), and ^{208}Th (as a proxy for Th) (Bunker and Bush, 1966, 1967; Aitken, 1985).

Sampling subsets (multiple small samples around an OSL site) were compared against each other in order to detect any heterogeneous subsurface conditions (*i.e.*, large stones, clay layers, or incomplete cementation) as well as to fully account for any gamma activity that the OSL sample received from layers above and below where different grain sizes or sources were a potential issue. The bulk samples were dried, homogenized by gentle disaggregation, weighed, sealed in plastic planchets with a diameter of 15.2 cm × 3.8 cm (a slight modification from Murray et al., 1987; Snyder and Duval, 2003), and then immediately placed in a gamma-ray spectrometer for ~8.5 h. Samples were then stored for at least 21 days to allow radon to achieve radioactive equilibrium, and the gamma-ray spectrometric measurements were repeated. The fraction of radon emanation was estimated from the difference of these two spectrometer measurements. A sealed/unsealed ratio of <1.10 is considered to represent negligible escape of radon under

laboratory conditions. Further details and comparisons are in the on-line Supplemental information section (Tables S.5 and S.6).

Luminescence age calculations

Water content and the effect on dose rate calculations were determined using methods described by Mahan et al. (2007) and Owen et al. (2007). We assumed that the samples were continuously saturated since burial, which is supported by sedimentological evidence and field observations. Ages are presented in “calendar” years before present (0 yr = AD 2011) and uncertainties are given at the 95% (2σ) confidence level in contrast to traditional reported values in the luminescence literature which are usually given at the 68% (1σ) level.

Results and discussion

Radiocarbon

Both ABA-treated and untreated aliquots of wood collected from the Main Silt at Locality 75 yielded “infinite” radiocarbon ages, *i.e.*, ages indistinguishable from background levels (Table 1). Similarly, all but two of the organic samples collected from the main exposures at localities 43, 51, and 52 yielded infinite radiocarbon ages. The ^{14}C activities of the other two samples, ZR10.52.9a (−39) and ZR10.52.8 (−123), differed from background by less than three sigma. We interpret these as minimum ages because very small amounts of persistent exogenous matter can easily produce such near-infinite ages from radiocarbon-dead material, and incomplete removal of such trace amounts of contaminants cannot be precluded.

Both treated and untreated aliquots of wood from the White Clay near the top of the sedimentary sequence at Locality 75 yielded finite ages (ZR11.ALJW.1, 44.5 ± 1.6 and 43.6 ± 1.4 cal ka BP, respectively). Unlike the results described above, the measured ^{14}C activities of these samples were significantly higher than identically treated blank material. The similarity in ages between the treated and untreated aliquots suggests that contamination is likely negligible and, therefore,

we view these ages as valid. However, we cannot extrapolate the ages between Locality 75 and sediments toward the center of the basin because the intervening material was removed prior to our arrival on site in October 2010.

Gastropod shell fragments collected from Unit 18 yielded an uncalibrated ^{14}C age of 44.3 ± 1.9 ^{14}C ka BP and collagen from dentin of the Clay Mammoth yielded an uncalibrated ^{14}C age of 46.2 ± 1.9 ^{14}C ka BP, both of which are beyond the limit of calibration. As with the near-infinite ages for the organic samples above, and for the same reasons, we interpret these as minimum (and most likely infinite) ages.

The organic component of untreated bone powder from the Clay Mammoth radius yielded an apparent age of 20.8 ± 0.45 cal ka BP. The base-soluble fraction (mostly humic acids) dated to $22.6 \pm 0.37/23.2 \pm 0.06$ cal ka BP based on multiple intercepts that were permitted during calibration (Table 1). The elemental compositions of these two samples indicate that little, if any, of the organic carbon present is from the original bone. Rather, it appears to be a mixture of microbial remnants and humic acids introduced after the animal died. Thus, these ages should be viewed as *minima* and are obviously much younger than the true age of the Clay Mammoth, although how much younger cannot be determined by the ^{14}C data alone. In sum, nearly all of the ages obtained by radiocarbon dating appear to be either compromised by contamination or are beyond the limit of the technique.

In situ cosmogenic radionuclides

Based on the “global” production rate coded in the CRONUS calculator and the measured ^{10}Be and ^{26}Al concentrations given in Table 2, we calculated exposure ages of 138 ± 12 ka and 129 ± 12 ka, respectively, for sample ZR11-BLO. We also evaluated model ages using a “regional” ^{10}Be production rate for northeastern North America (Balco et al., 2008), which is more consistent with many of the production-rate estimates generated recently that are ~5–10% lower than the global values (*e.g.*, Putnam et al., 2010; Goehring et al., 2011; Kaplan et al., 2011; Briner et al., 2012). Predictably, ages calculated using the lower

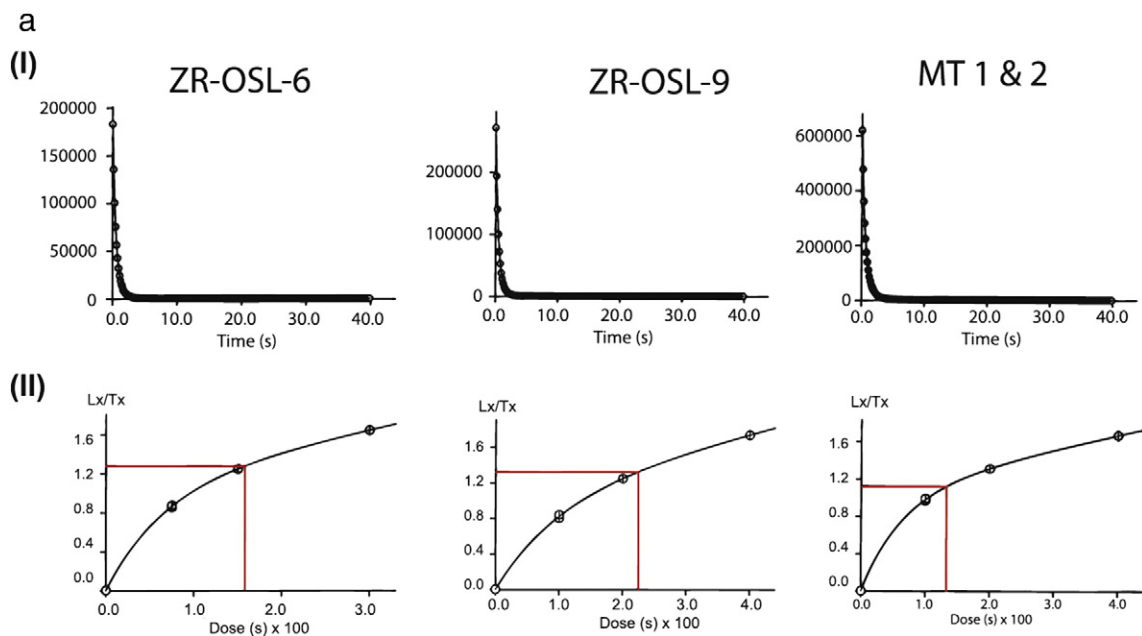


Figure 6. (a) Decay curves for OSL analysis of samples ZR11-OSL-6, ZR11-OSL-9, and MT1&2. Samples were analyzed following the SAR protocol on aliquots of 90–63 μm quartz grains (Murray and Wintle, 2003). OSL decay curves demonstrate a dominant fast component and little to no medium or slow component when subjected to blue light stimulation. All OSL samples from the ZRFS demonstrated this behavior, which we interpret as mature quartz (multiple bleach/dose cycles) with no significant feldspar contamination. (b) OSL growth curves are best fit with a linear + exponential regression and demonstrate recycle ratios of approximately 1.0. The curve shape and recycle ratios suggest that the quartz has not reached saturation, nor is thermal transfer present. Characteristics of the OSL signal are quite similar despite differences in equivalent dose dispersion.

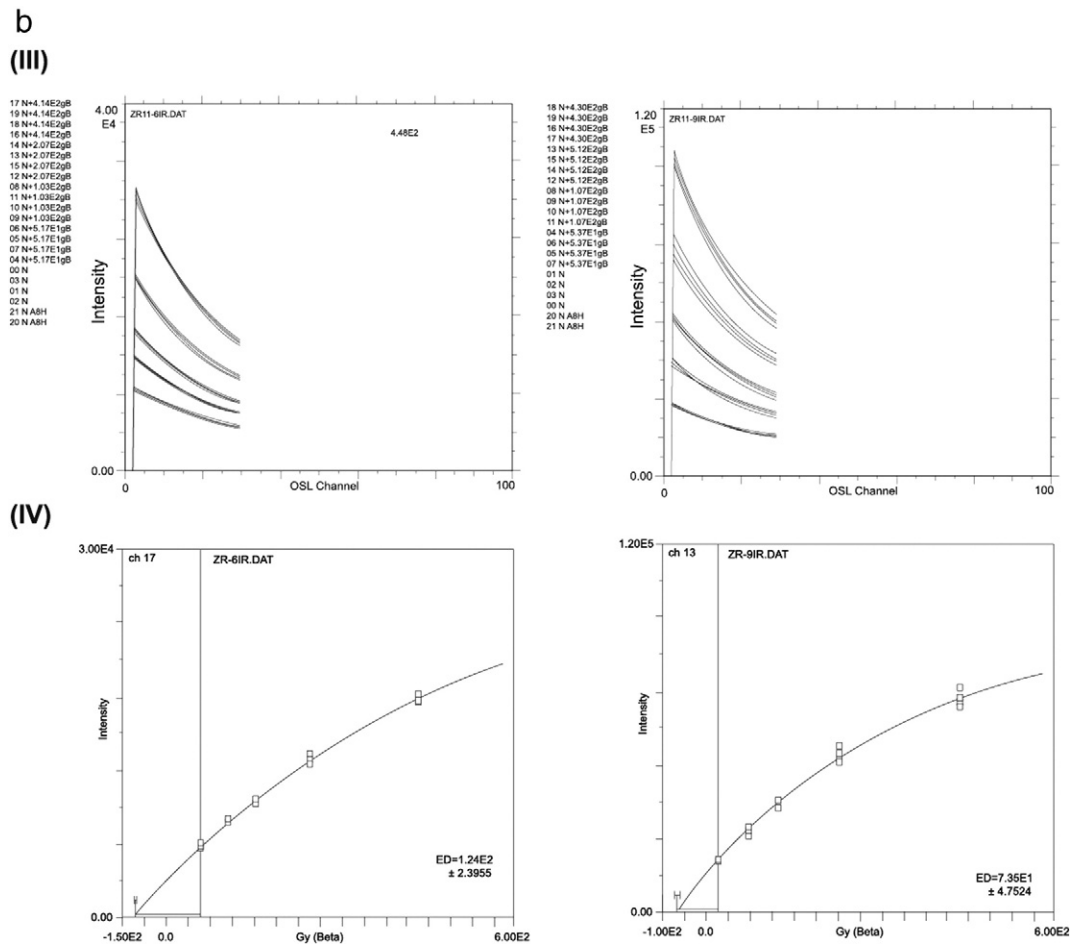


Figure 6 (continued).

“regional” production rates are older than those derived with the global values: 158 ± 9 ka for ^{10}Be and 149 ± 9 ka for ^{26}Al (Table 2 and Supplemental Table S.2).

Regardless of which production rate or scaling model is used, the calculated ages should be viewed as *minimum* ages since any erosion effects (which would increase the exposure age if considered explicitly) are neglected. The ratio of concentrations of ^{10}Be to ^{26}Al is 6.15 ± 0.23 , somewhat below the generally accepted production ratio of 6.75 (Balco and Shuster, 2009). When plotted on a two-isotope diagram, the sample and its 68% (1σ) confidence interval lie in the burial or complex exposure (exposure, burial, re-exposure) field but overlap the continuous exposure with the steady erosion field. The sample is not distinguishable from the line of continuous exposure with no erosion at the 95% (2σ) confidence level (Supplemental Fig. S.2). Because a surface exposure age of a single sample does not allow us to evaluate issues related to inheritance or burial, we cannot confidently choose one scenario (continuous exposure *versus* episodic burial) over the other.

^{10}Be and ^{26}Al analytical results for the depth profile samples are presented in Supplemental Table S.3. We followed Goehring et al. (2010) and fit an exponential profile for nucleon spallation to the data for each nuclide, since spallation production dominates at the high site altitude and shallow depths sampled here. We then compared the projected surface concentrations to those from the surface boulder, for a range of assumed mean profile bulk densities (2.2 to 2.7 g cm^{-3}) (Supplemental Table S.4). Predicted results are not particularly sensitive to the assumed bulk density (Supplemental Figs. S.3 and S.4). Model fits indicate no significant inheritance in the profile for either nuclide, while projected surface concentrations are ca. 30% of the respective surface

boulder measured nuclide concentrations – corresponding exposure ages are comparably low (Supplemental Table S.4). Assuming that the surface boulder concentrations represent a simple exposure scenario (*i.e.*, no inheritance, no significant erosion of the boulder surface, no burial and re-exposure), this suggests erosion of the moraine crest during continuous exposure of the boulder at the surface, consistent with the boulder’s geomorphic setting on a broad, lower elevation portion of the crest. We then modeled the range of predicted erosion depths to bring the projected profile surface concentrations into agreement with the surface boulder for both nuclides, assuming 160 g cm^{-2} for the spallogenic attenuation length. Results suggest a minimum of ca. 70 ± 8 cm of erosion for the moraine crest during the boulder exposure period, yielding a moraine crest erosion rate of at least ca. 4–6 mm/ka. This supports our interpretation of the surface boulder exposure age as a minimum.

Uranium-series

U concentrations in bone specimens ranged from 0.0015 to 8.60 $\mu\text{g/g}$ (ppm) with a median value of 0.053 $\mu\text{g/g}$. Many specimens have concentrations consistent with the low values present in living bone tissue, reflecting the limited secondary mobility of U under the anoxic conditions characteristic of the site. Profiles across several samples of thick, compact bone did not show U-shaped concentration profiles that are common in bone from environments where substantial U uptake has occurred (Pike et al., 2002). Th concentrations also span a wide range from 0.0068 to 11.2 $\mu\text{g/g}$ with a median value of 0.111 $\mu\text{g/g}$. Consequently, many samples had high Th/U ratios that were unfavorable for obtaining precise U-series ages. Only a small number of analyses

allowed calculation of finite $^{230}\text{Th}/\text{U}$ ages with reasonably small uncertainties (Fig. 4). Even these must be viewed with caution because of the likelihood of secondary U mobility.

A set of criteria was established for determining which analyses preserved useful U-series geochronological information. In order to calculate Th-corrected U-series compositions and viable $^{230}\text{Th}/\text{U}$ ages, samples first had to contain sufficient U to obtain reliable analytical results. Analyses with U concentrations $>0.05 \mu\text{g/g}$ were considered necessary to yield robust ^{234}U and ^{230}Th measurements and not be overly susceptible to compromise from laboratory blanks or small amounts of geological variability. Secondly, detrital Th must be low enough to avoid large corrections and increased uncertainties propagated from the unknown detrital component.

Although all analyses have similar analytical errors on measured ratios, those with the lowest $^{232}\text{Th}/^{238}\text{U}$ AR (<0.3) or highest $^{230}\text{Th}/^{232}\text{Th}$ AR (>3) yield calculated ages that are the least dependent on correctness of the assumed composition of the detrital component and yield the smallest age uncertainties. A final test of the viability of a calculated age is whether or not the initial $^{234}\text{U}/^{238}\text{U}$ AR value derived from the calculated $^{230}\text{Th}/\text{U}$ age and measured $^{234}\text{U}/^{238}\text{U}$ AR are consistent with U isotope compositions observed in groundwater incorporated into the bone. Because Th is insoluble under near-surface conditions, open-system chemical behavior involves gains or losses of U from the bone, resulting in erroneously low or high estimates of the $^{230}\text{Th}/^{238}\text{U}$ AR (movement of compositions along sub-horizontal trajectories on a U-series isotope evolution plot such as Fig. 4).

Only a small number of analyses meet these criteria and provide independent age information that helps constrain the history of the site. Detailed results for samples that either did not contain sufficient U, exhibited evidence of open-system behavior with respect to U, or yielded indeterminate ages are provided in Table 3.

Detritus-corrected U-series isotope compositions were calculated for two aliquots obtained from a bison femur present in Unit 15; however, the aliquot with the lower U concentration, 60679a, has excess ^{230}Th indicating open-system behavior. The other sample, 60679b, has higher U (0.146 $\mu\text{g/g}$) and gives a $^{230}\text{Th}/\text{U}$ age of 49 ± 7 ka. The initial $^{234}\text{U}/^{238}\text{U}$ AR of 1.55 ± 0.04 obtained for this analysis is statistically identical to the value obtained for groundwater from the upper stratigraphic units.

Specimens from the main silt include a sample consisting of multiple salamander vertebrae, as well as a fragment of bison horn core. The salamander vertebrae (54.260) have elevated U and Th concentrations attributed to incomplete removal of fine detritus. However, this sample requires relatively small corrections for detrital Th and gives a ^{230}Th age of 73 ± 11 ka and viable initial $^{234}\text{U}/^{238}\text{U}$ AR (Fig. 4). A similar age of 75 ± 26 ka was obtained for one of two aliquots of a horn core fragment (48.018a). The other (48.018b) yielded a younger age of 47 ± 3 ka. Both aliquots have elevated U concentrations that suggest post-mortem U uptake. Thus, differences in ages for the two aliquots from the same bone fragment are attributed to different patterns of U diffusion and uptake. The younger aliquot is interpreted to represent more recent incorporation of U whereas the older date more closely approaches the age of burial. The best estimate for the minimum age of the

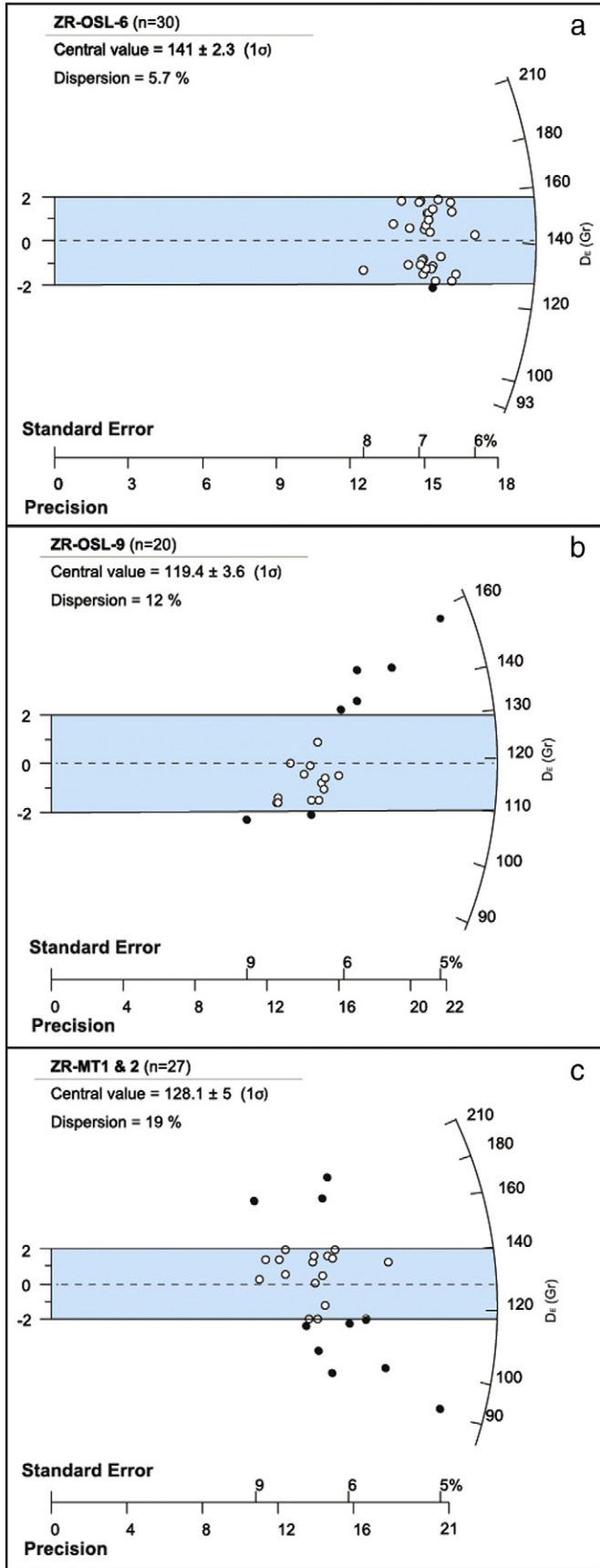


Figure 7. (a) Radial plot of equivalent dose measurements for sample ZR11-OSL-6 ($n = 30$). Radial plot indicates that the best fit is at about 140 Gray (Gy) and the weighted mean indicates a best fit at 139 Gy. There is very little scatter and the equivalent dose errors are all better than 8% while the over-dispersion of the equivalent doses is better than 9%. All grain sizes from 180 to 63 μm were combined to get enough quartz grains to analyze. (b) Radial plot of equivalent dose measurements for sample ZR11-OSL-9 ($n = 20$). Radial plot indicates that the best fit is at about 115 Gy and the weighted mean indicates a best fit at 114 Gy. There appears to be a minor trend to partial bleaching (note the scatter of equivalent doses higher than 120 Gy). All grain sizes from 180 to 63 μm were combined to get enough quartz grains to analyze. (c) Radial plot of equivalent dose measurements for sample ZR-MT1&2 (DMNS #76.98), which was composed of sediments collected outside and adjacent to tusk ($n = 27$). Radial plot indicates that the best fit is at about 125 Gy and the weighted mean indicates that the best fit is at 117 Gy. However, there is substantial scatter in this sample and a trend from smaller equivalent doses that we attribute to light exposure during the collection of the bones. The dispersion is higher due to the effect of the scatter in the measured equivalent doses (at $>20\%$). All grain sizes from 250 to 63 μm were combined to get enough quartz grains to analyze for this sample only.

Table 4
Summary of OSL ages.

Sample ID	Unit	Locality	K (%) ¹	U (ppm) ¹	Th (ppm) ¹	Cosmic dose addition (Gy/ka) ²	Total dose rate (Gy/ka) ³	Equivalent dose (Gy) ³	n ⁴	Scatter (%) ⁵	OSL age (ka) ⁶
ZR12-87-2	18	87	1.86 ± 0.03	3.36 ± 0.07	9.65 ± 0.28	0.26 ± 0.02	1.83 ± 0.04	105 ± 3	25 (25)	12.2	57 ± 4
ZR12-87-1	18	87	1.86 ± 0.03	3.36 ± 0.07	9.65 ± 0.28	0.26 ± 0.02	1.83 ± 0.04	106 ± 3	28 (28)	12.9	58 ± 4
ZR12-87-3	18	87	1.54 ± 0.03	2.62 ± 0.14	7.88 ± 0.32	0.26 ± 0.02	1.52 ± 0.04	93 ± 3	19 (20)	12.0	61 ± 5
ZR12-87-4	18	87	1.54 ± 0.03	2.62 ± 0.14	7.88 ± 0.32	0.26 ± 0.02	1.52 ± 0.04	99 ± 4	20 (20)	8.9	65 ± 6
ZR11.OSL-9	17	51	1.57 ± 0.01	3.49 ± 0.12	8.38 ± 0.29	0.24 ± 0.02	1.64 ± 0.06	114 ± 5	20 (20)	14.2	70 ± 8
ZR11.OSL-6	14 (top)	43	1.69 ± 0.02	3.05 ± 0.09	8.73 ± 0.27	0.22 ± 0.02	1.64 ± 0.06	139 ± 5	30 (30)	8.9	85 ± 9
ZR11.OSL-5	14 (base)	43	1.82 ± 0.02	3.30 ± 0.10	9.03 ± 0.31	0.21 ± 0.02	1.73 ± 0.06	134 ± 5	30 (30)	8.8	77 ± 8
ZR11.OSL-4	13 (top)	43	1.89 ± 0.02	3.53 ± 0.10	9.34 ± 0.35	0.20 ± 0.02	1.78 ± 0.06	153 ± 8	20 (20)	8.5	86 ± 10
ZR11.OSL-3	13 (base)	43	1.72 ± 0.02	3.17 ± 0.09	8.42 ± 0.24	0.19 ± 0.02	1.62 ± 0.06	128 ± 5	30 (30)	12.8	79 ± 8
ZR11.OSL-2	10	43	1.84 ± 0.02	3.51 ± 0.10	8.42 ± 0.26	0.18 ± 0.02	1.71 ± 0.06	157 ± 6	30 (30)	10.7	92 ± 10
ZR11.OSL-11	10	- ⁷	1.84 ± 0.02	3.55 ± 0.12	8.53 ± 0.34	0.19 ± 0.02	1.72 ± 0.07	172 ± 7	30 (30)	9.2	100 ± 12
ZR11.OSL-10	10	- ⁸	1.49 ± 0.01	2.65 ± 0.09	6.40 ± 0.26	0.22 ± 0.01	1.42 ± 0.06	149 ± 8	20 (20)	10.6	105 ± 14
ZR11.OSL-1	9	43	1.84 ± 0.02	3.69 ± 0.11	8.42 ± 0.25	0.18 ± 0.02	1.76 ± 0.06	171 ± 6	28 (28)	10.7	97 ± 10
ZR11.OSL-7	9a	52	1.95 ± 0.02	3.66 ± 0.13	8.95 ± 0.35	0.17 ± 0.01	1.78 ± 0.07	201 ± 10	29 (30)	4.6	113 ± 14
ZR11.OSL-8	8	52	1.91 ± 0.02	4.08 ± 0.14	8.10 ± 0.32	0.16 ± 0.01	1.76 ± 0.07	238 ± 9	25 (25)	15.8	135 ± 15
Deep Pit-4.5	6 ⁹	-	2.09 ± 0.04	3.42 ± 0.19	8.31 ± 0.21	0.07 ± 0.01	1.69 ± 0.07	200 ± 6	30 (31)	10.5	118 ± 12
MT-1a	5	-	1.53 ± 0.03	2.08 ± 0.07	6.93 ± 0.13	0.10 ± 0.01	1.36 ± 0.03	160 ± 4	27 (27)	8.1	118 ± 8
MT-1b	5	-	2.07 ± 0.08	3.04 ± 0.20	7.73 ± 0.48	0.10 ± 0.01	1.74 ± 0.06	213 ± 7	24 (26)	14.3	122 ± 12

Note: Uncertainties for all dose parameters and ages are given at the 2σ (95%) confidence level.

Additional information for ages used in depth modeling may be found in Supplemental information.

¹ Analyses obtained using ICP-MS. All are total digests with HF and HNO₃. Equilibration was done with 9 N HCl.

² Cosmic doses and attenuation with depth were calculated following Prescott and Hutton (1994). See text for details.

³ Dose rate and equivalent dose for fine-grained 180–90 μm quartz sand at 100% water content. Linear + exponential fit on equivalent dose, with single aliquot regeneration.

⁴ Number of replicated (De) estimates used to calculate the mean. Figures in parentheses indicate total number of measurements made including failed runs with unusable data.

⁵ Defined as “over-dispersion” of the De values. Obtained by taking the average over the std deviation. Values < 15% are considered to be well bleached sediments.

⁶ OSL ages are calculated by dividing the equivalent doses by the Dose Rates.

⁷ Sample OSL-11 was collected ~20 m south of Locality 43.

⁸ Sample OSL-10 was collected ~20 m north of Locality 43.

⁹ This unit designation is most likely correct but could not be verified in the field because of safety concerns. Therefore it was excluded from the BACON age–depth model.

Main Silt based on U-series data is interpreted as 73 ± 10 ka based on the weighted mean of ages for specimens 54.260 and 48.018a.

Specimens from the Basement Silt include a small fragment from a rabbit femur (76.127) and a mastodon tooth including enamel and dentine (82.148). The rabbit femur has an elevated U concentration of 2.39 μg/g and a very favorable ²³⁰Th/²³²Th AR of 37.2. The resulting ²³⁰Th/U age of 104 ± 2 ka requires negligible correction for initial ²³⁰Th. Furthermore, the initial ²³⁴U/²³⁸U AR of 1.623 ± 0.008 is statistically identical to the value from 48.018a giving increased confidence that the U in both specimens evolved under closed-system conditions after initial U uptake. In contrast, samples of the mastodon tooth have U concentrations that are either extremely low (0.001 and 0.009 μg/g for enamel) or show evidence of open-system behavior (Fig. 5).

Aliquots of dentine form a horizontal array with variable ²³⁰Th/²³⁸U AR and measured ²³⁴U/²³⁸U AR values that project back to the value for the 104 ka rabbit femur. These data are consistent with patterns of recent U loss from material having a similar age as the rabbit femur. Given these facts, the age of 171 ± 11 ka from the mastodon tooth, as shown calculated in Table 3, is interpreted as an artifact of recent U mobility, and the best estimate of the minimum age for the basement silt is 104 ± 2 ka.

Luminescence

A total of 18 luminescence samples were collected at the ZRFS, including lacustrine sediments exposed in outcrop (n = 11), sediments trapped within mammoth and mastodon tusks recovered from the Main Silt (n = 2), and blocks of sediment from Unit 18 at Locality 87 (n = 4) and from Unit 6 exposed in a deep pit east of Locality 43 (n = 1) (Fig. 2). These samples span deposition of units 5 through 18, which constitute ~90% of the stratigraphic column at the site. Nearly all of the quartz in the samples show evidence that the grains were bleached prior to deposition and produced D_E distributions that exhibit < 15% over-dispersion (scatter), which is unusually good for an alpine lake setting (Figs. 7a, b, and c; Lang, 1994; Fuchs and Owen, 2008).

We did not have a modern analog sample for the lake sediment since the surrounding lake basin and overlying material had been either very heavily modified or removed prior to the arrival of scientists at the site. However, since fluvial input to the lake was likely minimal (see Pigati et al., 2014), accumulation of eolian sediments would have been interrupted occasionally by the near-shore slumps that consisted of reddish-brown coarse sediments as compared to the mostly gray, fine-grained lacustrine material. We did not sample for OSL anywhere near the debris flows. We were also concerned about ice as a factor in the amount of luminescence the sediment was able to receive during burial, but we did not observe any evidence of ice wedges or ice-wedge casts that would indicate continuous permafrost (Bateman, 2008).

The OSL ages ranged from 122 ± 12 to 57 ± 4 ka, excluding a single sample (ZR11.OSL-8) which gave an anomalously old age of 135 ± 15 ka near the middle of the stratigraphic section (Table 4). Overall, the luminescence ages maintain stratigraphic order throughout the sedimentary sequence, fall within the bounds established by the ¹⁴C and cosmogenic dating results, overlap the most credible U-series age on the rabbit femur, and demonstrate that the fossil-bearing lake sediments span the latest part of Marine Oxygen Isotope Stage (MIS) 6, all of MIS 5 and MIS 4, and the early part of MIS 3.

Despite their antiquity, we view the OSL ages as robust and reliable for several reasons. First, we determined the dose rates using multiple techniques both in the field and laboratory, which were consistent between the methods and show very little to no disequilibrium within the lake sediments themselves (Supplemental Table S.6). We also stayed away from sampling near peat because disequilibrium has been previously documented for that particular material (Duller, 2008).

Second, the sedimentary units that we sampled at localities 43, 51, and 52 were located near the center of the lake, and were massive and homogenous, which maximizes the accuracy of the dose rate determination. The measured dose rates (1.4–1.8 Gy/ka) were also low enough that the growth of the luminescence signal was slow, steady, and apparently undisturbed (Table 4).

Third, dispersion of the D_E's were quite low (or highly symmetrical), generally < 15%, which leads to a more precise determination of the final

ages because the random errors (variation in the brightness of D_E in grains, assessing the sensitivity of the D_E signal, assumptions regarding the form of the dose–response, errors in individual L/T ratios, and transforming the error in the L/T ratios to an error in D_E) and systematic errors (water content of the sediment over time, cosmic dose component that varies with elevation and depth over time, errors in the calibration of the gamma or beta sources used to irradiate the sample, or suitability of the sediment (or material) for use with the single-aliquot regeneration procedure) (Duller, 2007) associated with calculating an OSL age are small (Fuchs and Wagner, 2003; Lepper et al., 2011). Traditionally, uncertainties arising from systematic errors tend to be swamped by those arising from random errors, especially errors associated with measurement of D_E values (Duller, 2007; Lepper et al., 2011). The propagated age uncertainty (Aitken, 1985), which takes geological uncertainties into consideration and is the traditional method of error reporting for OSL dating, is therefore also small.

Finally, quartz grains deposited in the lake appear to be largely eolian and fully bleached (see Supplemental Table S.5). This is ideal in terms of dating as the majority of the sampled grains were bleached distally, prior to deposition, in spite of the proximal glacial environment and climate at the ZRFS during lake sediment formation. Our reconstructed scenario puts the burial of the quartz and fine-grained silt in the best possible post-depositional conditions for the OSL technique: fully bleached prior to deposition

but entombed under perpetually dark, cold, non-bioturbated, and homogeneous sedimentation.

Age–depth model

The OSL dates were used to produce a Bacon age–depth model (Bayesian accumulation histories for deposits) that aims to model flexible accumulation rates (Blaauw and Christen, 2011). The Bacon model can work with radiocarbon dates as well dates on the calendar scale, such as luminescence ages. Bacon divides a core into many thin vertical sections (default resolution 5 cm), and through millions of Markov Chain Monte Carlo (MCMC) iterations, estimates the accumulation rate (in yr/cm; so more correctly, sedimentation times) for each of these sections. Combined with an estimated starting date for the first section, these accumulation rates then form the age–depth model (Blaauw and Christen, 2011). The ZRFS sediments were divided into 52 vertical sections of 20 cm thickness each. Prior settings for the accumulation rates were prescribed by a gamma distribution with shape 1.1 and a mean of 100 yr/cm. Flexibility in the accumulation rate between neighboring depths (memory) was steered by a Beta distribution with default parameters using a strength of 4 and a mean value of 0.7 (Figs. 8a–d).

OSL ages in units 13 and 14 did not change significantly with depth and, therefore, it was necessary to assign independent ages

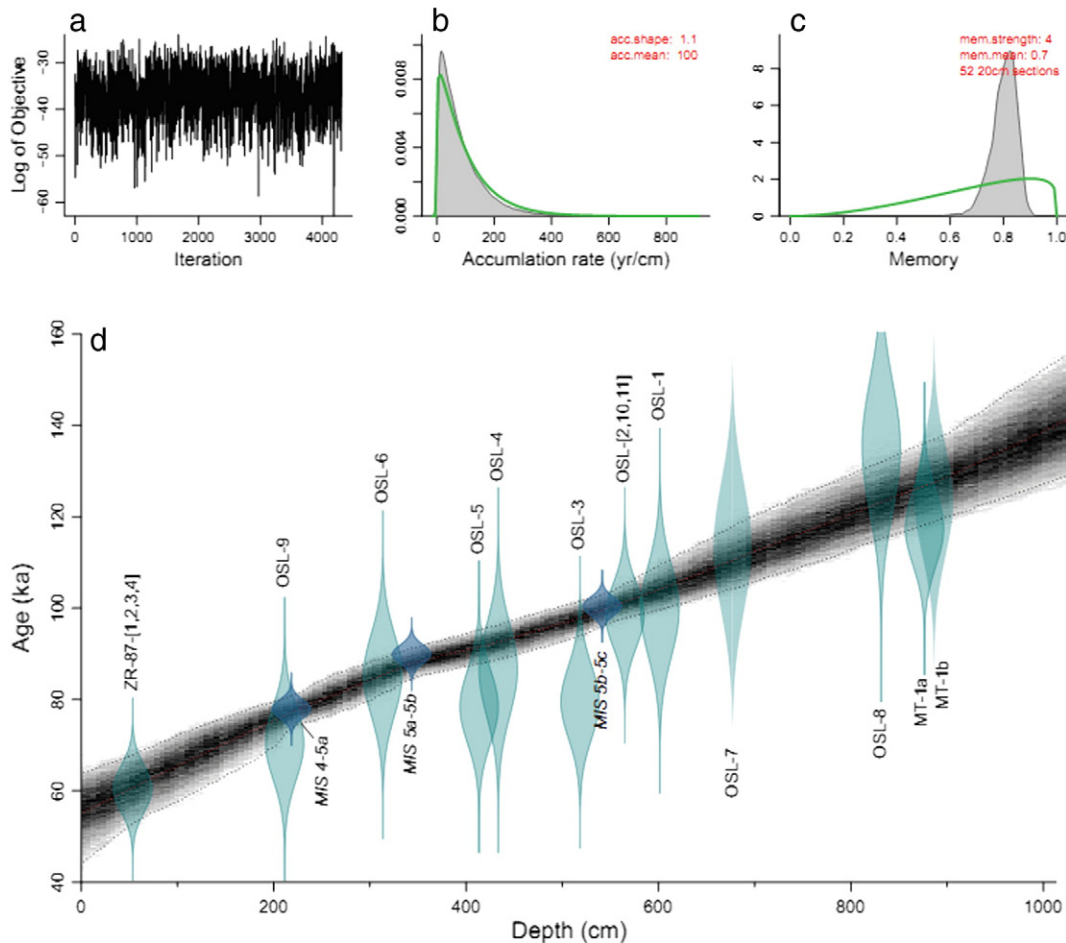


Figure 8. The inset panels at the top show (a) the number of Markov Chain Monte Carlo (MCMC) iterations used to generate the gray-scale graphs, (b) the prior (green) and posterior (gray) distributions of accumulation rates, and (c) the prior (green) and posterior (gray) distributions of memory. The main panel (d) shows the posterior age–depth results of Bacon modeling (gray), individual OSL ages (light green), and the three ages derived from correlating the ZRFS pollen record and marine isotope stages (light blue). Gray dots indicate the model's 95% probability intervals. Note that sample ZR-87-[1, 2, 3, 4] represents the average of four OSL ages obtained from Unit 18. Similarly, sample OSL-[2, 10, 11] represents the average of three OSL ages obtained from Unit 10. All others represent individual OSL ages.

to these units based on changes in the ZRFS pollen spectra that appear to correlate with the transitions in the marine foraminifera records (Anderson et al., 2014—in this volume). The additional ages, depths, and inferred transitions were (1) 100 ka, 538 cm depth, MIS 5c–5b, (2) 89.5 ka, 340 cm depth, MIS 5b–5a, and (3) 77.5 ka, 215 cm depth, MIS 5a–4 (Murray et al., 1987). We assumed uncertainties of 2 ka (1 sigma) for each. These additions allow the model ages to increase with depth through these two units, and appear to be reasonable based on observed changes in other environmental proxy data (Elias, 2014—in this volume; Haskett and Porinchu, 2014—in this volume; Sharpe and Bright, 2014—in this volume; Strickland et al., 2014—in this volume). However, given the dangers of circularity when including relative ages to an otherwise independent chronology (Blaauw, 2012), we refrain from any subsequent interpretation of climate leads or lags for this time period. The final Bacon age – depth model (Fig. 8d) agrees well with the OSL and pollen-based ages, showing no outliers and good mixing of MCMC iterations.

Conclusions

The results of four independent chronometric techniques, including ^{14}C , cosmogenic surface exposure dating, U-series, and luminescence, show that the ages of sediments at the ZRFS span the end of MIS 6, all of MIS 5 and MIS 4, and the earliest part of MIS 3. Radiocarbon and *in situ* cosmogenic radionuclides placed limits on the upper (>45 ka) and lower portions (~130 ka) of the sedimentary sequence, respectively. A small number of samples met the criteria for U-series dating that allowed calculation of viable ages for three stratigraphic units: 49 ± 7 ka for Unit 15, 73 ± 11 ka for the Main Silt, and 104 ± 2 ka for the Basement Silt. Although the $^{230}\text{Th}/\text{U}$ age results maintain stratigraphic consistency and fall with the bounds set by radiocarbon and cosmogenic radionuclide dating, low U concentrations and evidence of open-system behavior with respect to uranium limit the utility of these ages.

Luminescence dating (specifically quartz OSL) yielded robust and reliable ages for the bulk of the sedimentary sequence at the site. Although it is often difficult to obtain old (>100 ka) luminescence ages due to issues with sources, transport mechanisms, and preservation potential, our results demonstrate that several components fortuitously merged at the ZRFS. First, dose rates were sufficiently low to avoid saturation of the luminescence signal. Second, the narrow equivalent dose distributions of the samples analyzed indicate that the sampled sediments likely were transported into the lake basin *via* eolian processes, which is ideal for luminescence dating. Finally, sediments were largely homogenous and non-bioturbated, meaning there was little chance for post-burial exposure of the sample sediments.

The SAR protocol used in this study is optimal for dating the ZRFS samples based on the results of multiple quality control tests, including the recycling ratio, recuperation, IR repeat ratio, dose recovery, preheat plateau, and the $D_E(t)$ distribution measurements. Low skewness, overdispersion, and rate of luminescence accumulation, along with an amenable transport mechanism of the sampled sediments and the homogenous nature of the lake sediments, give us confidence in the final OSL ages. Moreover, the ages maintain stratigraphic order throughout the sedimentary sequence and fall within the bounds established by ^{14}C and cosmogenic surface exposure ages. Ages for specific fossil localities can be extrapolated to the sampled units using stratigraphic correlation. The Bacon age – depth model produced reasonable accumulation rates using OSL and pollen-based ages. Finally, in addition to establishing a chronological framework at the ZRFS, our study provides a temporal foundation for future studies of the last interglacial period in the Colorado Rockies.

Acknowledgments

The samples used in this study were collected with the kind help and support of Cayce Gulbransen and Tom Ager of the U.S. Geological Survey

and Carol Lucking of the Denver Museum of Nature and Science. The authors thank History Colorado/The Colorado Historical Society, the Snowmass Water and Sanitation District, and the Town of Snowmass Village for their assistance with this excavation. N. Lifton thanks Brent Goehring for ^{10}Be and ^{26}Al sample processing, and the PRIME Lab staff for the measurements. Specimens referenced in this paper were collected at the Ziegler Reservoir locality, 5PT1264, under State of Colorado Paleontological Permits 2010–106 and 2011–17. We thank Ben Laabs (SUNY Geneseo) and Regina DeWitt (ECU) for careful reviews that made this paper more cohesive and balanced. Finally, we thank bulldozer operator Jesse Steele for grasping the significance of what lay beneath his blade on that fateful afternoon of October 14, 2010.

Appendix A. Supplementary information

Supplementary data to this article can be found online at <http://dx.doi.org/10.1016/j.yqres.2014.03.004>.

References

- Aitken, M.J., 1985. Thermoluminescence Dating. Academic Press, London.
- Aitken, M.J., 1998. An Introduction to Optical Dating: The Dating of Quaternary Sediments by the Use of Photon-stimulated Luminescence. Oxford University Press, Oxford.
- Alexanderson, H., Murray, A.S., 2012. Problems and potential of OSL dating Weichselian and Holocene sediments in Sweden. Quaternary Science Reviews 44, 37–50. <http://dx.doi.org/10.1016/j.quascirev.2009.09.020>.
- Anderson, R.S., Jimenez-Moreno, G., Ager, T., Porinchu, D.F., 2014. High-elevation paleoenvironmental change during MIS 6–4 in Colorado's Central Rockies as determined from pollen an. Quaternary Research 82, 542–552 (in this volume).
- Balco, G., Shuster, D.L., 2009. ^{26}Al ^{10}Be ^{21}Ne burial dating. Earth and Planetary Science Letters 286 (3–4), 570–575. <http://dx.doi.org/10.1016/j.epsl.2009.07.025>.
- Balco, G., Stone, J.O., Lifton, N.A., Dunai, T.J., 2008. A complete and easily accessible means of calculating surface exposure ages or erosion rates from Be-10 and Al-26 measurements. Quaternary Geochronology 3 (3), 174–195. <http://dx.doi.org/10.1016/j.quageo.2007.12.001>.
- Bateman, M.D., 2008. Luminescence dating of periglacial sediments and structures. Boreas 37, 574–588. <http://dx.doi.org/10.1111/j.1502-3885.2008.00050.x>.
- Bateman, M.D., Swift, D.A., Piotrowski, J.A., Sanderson, D.C.W., 2012. Investigating the effects of glacial shearing of sediment on luminescence. Quaternary Geochronology 10, 230–236.
- Blaauw, M., 2012. Out of tune: the dangers of aligning proxy archives. Quaternary Science Reviews 36, 38–49.
- Blaauw, M., Christen, J.A., 2011. Flexible paleoclimate age – depth models using an autoregressive gamma process. Bayesian Analysis 6, 457–474.
- Blackwelder, E., 1915. Post-Cretaceous history of the mountains of central western Wyoming. Journal of Geology 23, 97–117 (193–217, 307–340).
- Briner, J.P., Young, N.E., Goehring, B.M., Schaefer, J.M., 2012. Constraining Holocene ^{10}Be production rates in Greenland. Journal of Quaternary Science 27 (1), 2–6. <http://dx.doi.org/10.1002/jqs.1562>.
- Bunker, C.M., Bush, C.A., 1966. Uranium, thorium, and radium analyses by gamma-ray spectrometry (0.184–0.352 million electron volts). U.S. Geological Survey Professional Paper 550-B, pp. B176–B181.
- Bunker, C.M., Bush, C.A., 1967. A comparison of potassium analyses by gamma-ray spectrometry and other techniques. U.S. Geological Survey Professional Paper 575-B, pp. B164–B169.
- Delanghe, D., Bard, D., Hamelin, B., 2002. New TIMS constraints on the uranium-238 and uranium-234 in seawaters from the main ocean basins and Mediterranean Sea. Marine Chemistry 80, 79–93.
- Duller, G.A.T., 2007. Assessing the error on equivalent dose estimates derived from single aliquot regenerative dose measurements. Ancient TL 25, 15–24.
- Duller, G.A.T., 2008. Luminescence Dating: Guidelines on Using Luminescence Dating in Archaeology. English Heritage, Swindon (45 pp.).
- Elias, S.A., 2014. Environmental interpretation of fossil insect assemblages from MIS 5 at Ziegler Reservoir, Snowmass, Colorado. Quaternary Research 82, 592–603 (in this volume).
- Fuchs, M., Owen, L.A., 2008. Luminescence dating of glacial and associated sediments: review, recommendations and future directions. Boreas 37, 636–659.
- Fuchs, M., Wagner, G.A., 2003. Recognition of insufficient bleaching by small aliquots of quartz for reconstructing soil erosion in Greece. Quaternary Science Reviews 22 (10–13), 1161–1167. [http://dx.doi.org/10.1016/S0277-3791\(03\)00039-8](http://dx.doi.org/10.1016/S0277-3791(03)00039-8).
- Galbraith, R.F., Green, P.F., 1990. Estimating the component ages in a finite mixture. Radiation Measurements 17, 197–206.
- Galbraith, R.F., Roberts, R.G., Laslett, G.M., Yoshida, H., Olley, J.M., 1999. Optical dating of single and multiple grains of quartz from Jinmium Rock Shelter, northern Australia, part 1: experimental design and statistical models. Archaeometry 41, 339–364.
- Goehring, B.M., Kelly, M.A., Schaefer, J.M., Finkel, R.C., Lowell, T.V., 2010. Dating of raised marine and lacustrine deposits in east Greenland using beryllium-10 depth profiles and implications for estimates of subglacial erosion. Journal of Quaternary Science 25, 865–874.

- Goehring, B.M., Mangerud, J., Svendsen, J.I., Schaefer, J.M., Finkel, R.C., 2011. Late glacial and Holocene ^{10}Be production rates for western Norway. *Journal of Quaternary Science* 27 (1), 89–96. <http://dx.doi.org/10.1002/jqs.1517>.
- Gosse, J.C., Phillips, F.M., 2001. Terrestrial in situ cosmogenic nuclides: theory and applications. *Quaternary Science Reviews* 40 (14), 1475–1560.
- Haskett, D.R., Porinchu, D.F., 2014. A quantitative midge-based reconstruction of mean July air temperature from a high-elevation site in central Colorado, USA, for MIS 6 and 5. *Quaternary Research* 82, 580–591 (in this volume).
- Hedges, R.E.M., 1981. Radiocarbon dating with an accelerator: review and preview. *Archaeometry* 23 (1), 3–18.
- Heisinger, B., Lal, D., Jull, A., Kubik, P., Ivy-Ochs, S., Neumaier, S., Knie, K., Lazarev, V., Nolte, E., 2002a. Production of selected cosmogenic radionuclides by muons 1. Fast muons. *Earth and Planetary Science Letters* 200 (3–4), 345–355.
- Heisinger, B., Lal, D., Jull, A., Kubik, P., Ivy-Ochs, S., Knie, K., Nolte, E., 2002b. Production of selected cosmogenic radionuclides by muons: 2. Capture of negative muons. *Earth and Planetary Science Letters* 200 (3–4), 357–369.
- Ivanovich, M., Harmon, R.S., 1992. Uranium-series Disequilibrium: Applications to Earth, Marine, and Environmental Sciences, second ed. Clarendon Press, Oxford, U.K. (910 pp.).
- Kaplan, M.R., Strelin, J.A., Schaefer, J.M., Denton, G.H., Finkel, R.C., Schwartz, R., Putnam, A.E., Vandergoes, M.J., Goehring, B.M., Travis, S.G., 2011. In-situ cosmogenic ^{10}Be production rate at Lago Argentino, Patagonia: implications for late-glacial climate chronology. *Earth and Planetary Science Letters* 309 (1–2), 21–32. <http://dx.doi.org/10.1016/j.epsl.2011.06.018>.
- Kohl, C., Nishiizumi, K., 1992. Chemical isolation of quartz for measurement of in-situ-produced cosmogenic nuclides. *Geochimica et Cosmochimica Acta* 56 (9), 3583–3587.
- Ku, T.-L., 2000. Uranium-series methods. *Quaternary Geochronology: Methods and Applications. Reference Shelf, 4. American Geophysical Union pp. 101–114.*
- Lal, D., 1991. Cosmic ray labeling of erosion surfaces—in situ nuclide production rates and erosion models. *Earth and Planetary Science Letters* 104 (2–4), 424–439.
- Lang, A., 1994. Infrared stimulated luminescence dating of Holocene reworked silty sediments. *Quaternary Science Reviews* 13 (5–7), 525–528.
- Lepper, K., Gorz, K.L., Fisher, T.G., Lowell, T.V., 2011. Age determinations for glacial Lake Agassiz shorelines west of Fargo, North Dakota, USA. *Canadian Journal of Earth Sciences* 48, 1199–1207.
- Lian, O.B., Roberts, R.G., 2006. Dating the Quaternary: progress in luminescence dating of sediments. *Quaternary Science Reviews* 25, 2449–2468.
- Licciardi, J.M., 2000. Alpine Glacier and Pluvial Lake Records of Late Pleistocene Climate Variability in the Western United States. Ph.D. Dissertation Oregon State University, Corvallis, Oregon (155 pp.).
- Lucking, C., Johnson, K.R., Pigati, J.S., Miller, I.M., 2012. Primary mapping, stratigraphic data and field methods for the Snowmastodon Project. Denver Museum of Nature and Science Technical Report #2012-04, pp. 1–102.
- Ludwig, K.R., 2003. User's manual for Isoplot 3.00 a geochronological toolkit for Microsoft Excel. Berkeley Geochronology Center Special Publication, No. 4 (73 pp.).
- Ludwig, K.R., Paces, J.B., 2002. Uranium-series dating of pedogenic silica and carbonate, Crater Flat, Nevada. *Geochimica et Cosmochimica Acta* 66, 487–506.
- Ludwig, K.R., Titterton, D.M., 1994. Calculation of $^{230}\text{Th}/\text{U}$ isochrones, ages, and errors. *Geochimica et Cosmochimica Acta* 58, 5031–5042.
- Mahan, S.A., Miller, D.M., Menges, C.M., Yount, J.C., 2007. Late Quaternary stratigraphy and luminescence geochronology of the northeastern Mojave Desert. *Quaternary International* 166, 61–78.
- Murray, A.S., Olley, J.M., 2002. Precision and accuracy in the optically stimulated luminescence dating of sedimentary quartz: a status review. *Geochronometria* 21, 1–16.
- Murray, A.S., Wintle, A.G., 2003. The single aliquot regenerative dose protocol: potential for improvements in reliability. *Radiation Measurements* 37, 377–381.
- Murray, A.S., Marten, R., Johnston, A., Martin, P., 1987. Analysis for naturally occurring radionuclides at environmental concentrations by gamma spectrometry. *Journal of Radioanalytical and Nuclear Chemistry* 115, 263–288.
- Nishiizumi, K., 2004. Preparation of ^{26}Al AMS standards. *Nuclear Instruments and Methods in Physics Research Section B: Beam Interactions with Materials and Atoms* 223, 388–392. <http://dx.doi.org/10.1016/j.nimb.2004.04.075>.
- Nishiizumi, K., Imamura, M., Caffee, M., Southon, J., Finkel, R.C., McAninch, J., 2007. Absolute calibration of ^{10}Be AMS standards. *Nuclear Instruments and Methods in Physics Research Section B: Beam Interactions with Materials and Atoms* 258 (2), 403–413. <http://dx.doi.org/10.1016/j.nimb.2007.01.297>.
- Ochs, M., Ivy-Ochs, S., 1997. The chemical behavior of Be, Al, Fe, Ca and Mg during AMS target preparation from terrestrial silicates modeled with chemical speciation calculations. *Nuclear Instruments and Methods in Physics Research Section B* 123, 235–240. [http://dx.doi.org/10.1016/S0168-583X\(96\)00680-5](http://dx.doi.org/10.1016/S0168-583X(96)00680-5).
- Owen, L.A., Bright, J., Finkel, R.C., Jaiswal, M.K., Kaufman, D.S., Mahan, S., Radtke, U., Schneider, J.S., Sharp, W., Singhvi, A.K., Warren, C.N., 2007. Numerical dating of a late Quaternary spit–shoreline complex at the northern end of Silver Lake Playa, Mojave Desert, California: a comparison of the applicability of radiocarbon, luminescence, terrestrial cosmogenic nuclide, electron spin resonance, U-series and amino acid racemization methods. *Quaternary International* 166, 87–110.
- Pierce, K.L., 2003. Pleistocene glaciations of the Rocky Mountains. *Developments in Quaternary Sciences* 1, 63–76.
- Pigati, J.S., Miller, I.M., Jonson, K.R., Honke, J.S., Carrara, P.E., Muhs, D.R., Skipp, G., Bryant, B., 2014. Geologic setting and stratigraphy of the Ziegler Reservoir fossil site, Snowmass Village, Colorado. *Quaternary Research* 82, 477–489 (in this volume).
- Pike, A.W.G., Hedges, R.E.M., Van Calsteren, P., 2002. U-series dating of bone using the diffusion–adsorption model. *Geochimica et Cosmochimica Acta* 66 (24), 4273–4286.
- Prescott, J.R., Hutton, J.T., 1994. Cosmic ray contributions to dose rates for luminescence and ESR dating: large depths and long-term time variations. *Radiation Measurements* 23, 497–500.
- Putnam, A.E., Schaefer, J.M., Barrell, D.J.A., Vandergoes, M., Denton, G.H., Kaplan, M.R., Finkel, R.C., Schwartz, R., Goehring, B.M., Kelley, S.E., 2010. In situ cosmogenic ^{10}Be production-rate calibration from the Southern Alps, New Zealand. *Quaternary Geochronology* 5 (4), 392–409. <http://dx.doi.org/10.1016/j.quageo.2009.12.001>.
- Reimer, P.J., Baillie, M.G.L., Bard, E., Bayliss, A., Beck, J.W., Blackwell, P.G., Bronk Ramsey, C., Buck, C.E., Burr, G.S., Edwards, R.L., Friedrich, M., Grootes, P.M., Guilderson, T.P., Hajdas, I., Heaton, T.J., Hogg, A.G., Hughen, K.A., Kaiser, K.F., Kromer, B., McCormac, F.G., Manning, S.W., Reimer, R.W., Richards, D.A., Southon, J.R., Talamo, S., Turney, C.S.M., van der Plicht, J., Weyhenmeyer, C.E., 2009. IntCal09 and Marine09 radiocarbon age calibration curves, 0–50,000 years cal BP. *Radiocarbon* 51 (4), 1111–1150.
- Rhodes, E.J., 2011. Optically stimulated luminescence dating of sediments over the past 200,000 years. *Annual Review of Earth and Planetary Sciences* 39, 461–488.
- Rhodes, E.J., Singarayer, J.S., Raynal, J.P., Westaway, K.E., Sbihi-Alaoui, F.Z., 2006. New age estimates for the Palaeolithic assemblages and Pleistocene succession of Casablanca, Morocco. *Quaternary Science Reviews* 25, 2569–2585.
- Rodnight, H., 2008. How many equivalent dose values are needed to obtain a reproducible distribution? *Ancient TL* 26 (1), 3–9.
- Sharpe, S.E., Bright, J., 2014. A high-elevation MIS 5 hydrologic record using mollusks and ostracodes from Snowmass Village, Colorado, USA. *Quaternary Research* 82, 604–617 (in this volume).
- Simms, A.R., DeWitt, R., Kouremenos, P., Drewry, A.M., 2011. A new approach to reconstructing sea levels in Antarctica using optically stimulated luminescence of cobble surfaces. *Quaternary Geochronology* 6, 50–60.
- Snyder, S.L., Duval, J.S., 2003. Design and construction of a gamma-ray spectrometer system for determining natural radioactive concentrations in geological samples at the U.S. Geological Survey in Reston, Virginia. U.S. Geological Survey Open-File Report 03–29 (on-line only, <http://pubs.usgs.gov/of/2003/of03-029/>).
- Stone, J., 2000. Air pressure and cosmogenic isotope production. *Journal of Geophysical Research* 105 (B10), 23,753–23,759.
- Strelow, F., Weinert, C., Eloff, C., 1972. Distribution coefficients and anion exchange behavior of elements in oxalic acid–hydrochloric acid mixtures. *Analytical Chemistry* 44 (14), 2352–2356.
- Strickland, L.E., Baker, R.G., Thompson, R.S., Miller, D.M., 2014. Last interglacial plant macrofossils and climates from Ziegler Reservoir, Snowmass Village, Colorado. *Quaternary Research* 82, 553–566 (in this volume).
- Stuiver, M., Reimer, P., 1993. University of Washington Quaternary Isotope Lab Radiocarbon Calibration Program Rev. 3.0.3A. *Radiocarbon* 35, 215–230.
- Watanabe, Y., Nakai, S., 2006. U–Th radioactive disequilibrium analyses for JCP-1, coral reference distributed by the Geological Survey of Japan. *Geochemical Journal* 40, 537–541.
- Wintle, A.G., Murray, A.S., 2006. A review of quartz optically stimulated luminescence characteristics and their relevance in single-aliquot regeneration dating protocols. *Radiation Measurements* 41, 369–391.